Content-Aware Cooperative Transmission in HetNets With Consideration of Base Station Height

Huici Wu, *Student Member, IEEE*, Ning Zhang, *Member, IEEE*, Zhiqing Wei, *Member, IEEE*, Shan Zhang, *Member, IEEE*, Xiaofeng Tao, *Senior Member, IEEE*, Xuemin Shen, *Fellow, IEEE*, and Ping Zhang

***Abstract*—With macrocell base stations (MBSs) providing basic coverage for mobile users, the multiple tiers of cache-enabled small-cell base stations (SBSs) can opportunistically form user-centric clusters to enhance network capacity through traffic offloading and cooperative transmission. In this paper, we investigate cooperative transmission in cache-enabled heterogeneous networks considering the impact of base station (BS) heights. Specifically, the user-centric cooperative SBS clusters are formed based on the information of the cached contents, the transmission distance, and the cell load at SBSs. The users failed to be offloaded to the cooperative SBS clusters are served by the nearest MBSs. By incorporating the COST 231 Hata model for the line-of-sight and nonline-of-sight channels, the explicit expressions for the average spectral efficiency (SE) are obtained with statistical characterizations for the cell load distribution, as well as the aggregated information and interference signal strength. The analytical results indicate that with the COST 231 Hata model and the cooperative SBS cluster, the average SE decreases with the increase of BS height. Moreover, different trade-offs exist with the varying cache size, SBS density, and cooperative distance threshold, which results in a bell-shaped SE with respect to (w.r.t) the SBS density and the cooperative distance threshold. In addition, with an appropriate cooperative distance threshold, the average SE exhibits a bell-shaped relationship w.r.t the cache size. Extensive simulations are conducted to validate the analytical results and demonstrate the impact of the network parameters.**

***Index Terms*—Cooperative transmission, cache, base station height, stochastic geometry.**

Manuscript received September 16, 2017; revised December 14, 2017; accepted January 30, 2018. Date of publication February 27, 2018; date of current version July 16, 2018. This work was supported in part by the National Key Research and Development Program of China under Grant 2017YFB0801702, in part by the National Natural Science Foundation of China under Grant 61701042 and Grant 61601055, in part by the Beijing Municipal Science and Technology Project under Grant D161100001016002, and in part by the Natural Sciences and Engineering Research Council of Canada. The review of this paper was coordinated by Dr. Y. Gao. *(Corresponding author: Xiaofeng Tao.)*

H. Wu and X. Tao are with the National Engineering Laboratory for Mobile Network Technologies, Beijing University of Posts and Telecommunications, Beijing 100876, China (e-mail: dailywu@bupt.edu.cn; taoxf@bupt.edu.cn).

N. Zhang is with the Department of Computing Science, Texas A&M University–Corpus Christi, Corpus Christi, TX 78412 USA (e-mail: Ning.Zhang@tamucc.edu).

Z. Wei and P. Zhang are with the Key Laboratory of Universal Wireless Communications, Ministry of Education, Beijing University of Posts and Telecommunications, Beijing 100876, China (e-mail: weizhiqing@bupt.edu.cn; pzhang@bupt.edu.cn).

S. Zhang is with the School of Computer Science and Engineering, Beihang University, Beijing 100191, China (e-mail: zhangshan2007@gmail.com).

X. Shen is with the Department of Electrical and Computer Engineering, University of Waterloo, Waterloo, ON N2L 3G1, Canada (e-mail: sshen@uwaterloo.ca).

Color versions of one or more of the figures in this paper are available online at http://ieeexplore.ieee.org.

Digital Object Identifier 10.1109/TVT.2018.2809616

I. Introduction

HETEROGENEOUS networks (HetNets) are seen as dominant network architecture in the next generation networks [1], [2] due to the seamless coverage and high network throughput. However, the densely deployed low-power small cell base stations (SBSs) along with the macrocell base stations (MBSs) can cause severe congestion in the backhaul network due to overhead signaling and information exchange among base stations (BSs), leading to high latency and reduced energy and spectral efficiencies. Employing the cache technologies at SBSs has great potential to alleviate the heavy burden on the backhaul links by storing popular contents at the network edge and serving mobile users (MUs) directly [3]–[6].

In HetNets with cache-enabled SBSs, the content placement and cell association are key issues for maximizing the network performance due to limited resources. Existing researches have studied various cache strategies and investigated the network performance in the cache-enabled HetNets [7]–[10]. Cooperative caching [11], [12] can enhance the occurrence of cache hit events by coordinating the cached popular contents at SBSs. [13] proved that coordinated multi-point (CoMP) transmission can significantly improve the cell edge performance in HetNets. Joint CoMP and caching in HetNets [14], [15] can further improve the coverage and capacity by coordinating multiple heterogeneous BSs and exploring collaborative content caching based on coordinated BS clusters and the corresponding network topology. Performance analysis in cache-enabled HetNets, with/without coordinated transmission, has also been conducted with stochastic geometry [12], [15]–[18].

However, two practical factors are seldom considered in existing works, including diverse BS heights and limited BS capacities. First, since the signal propagation in wireless media depends critically on the geographical environment, various BSs are placed at different locations and elevated at high infrastructures in practice, such as along the street in horizontal space, and on the roof of buildings in vertical plane, etc. The difference in heights among elevated BSs and between BSs and MUs affects the density and coverage area of BSs, which further influences the cache size of BSs and the cache placement strategies. Second, due to the limited resources (time, frequency and space) available at BSs, the BS capacity, i.e., the maximum number of MUs that can be simultaneously served by a BS, is constrained. The diverse height differences and constrained BS capacities,

along with the cache sizes of BSs, significantly affect the cell association and cell load distribution of a BS, which further have an impact on the design of CoMP transmission in cache-enabled HetNets. Therefore, we investigate the network performance of CoMP transmission in cache-enabled HetNets by considering the impact of height differences between BSs and MUs and constrained BS capacities.

In this paper, an MBS-assisted and content-aware cooperative transmission strategy is proposed to improve the transmission data rate with SBS offloading. Specifically, the multiple tiers of cache-enabled SBSs form user-centric SBS clusters to serve the MUs with cooperative transmission, being aware of the cached contents, the transmission distance and the cell load. MUs failed to be offloaded to the SBSs are served by the nearest MBSs. Considering the height differences between BSs and MUs, we analyze the average spectral efficiency (SE) with incorporation of line-of-sight (LoS) link and non-line-of-sight (NLoS) links. Firstly, the cell load distributions of MBSs and SBSs are analyzed. Then, the average SE is analytically obtained with statistical characterizations of both the aggregated information and interference signal strength. The analytical results find that the average SE decreases with the rise of the height difference. Moreover, with fixed height difference, several tradeoffs are revealed. Numerical and simulation results are provided to validate the theoretical analyses and to show the impact of the network parameters. The analyses reveal that the MBS-assisted and content-aware cooperative transmission can improve the SE performance by dynamically managing the size of cooperative SBS cluster and adjusting the network parameters, i.e., the BS height, the cache size of SBSs and the cooperative distance threshold. In a nutshell, The main contribution are summarized as follows:

- We propose the framework for the SE analysis in cache-enabled HetNets with cooperative transmission, considering the impact of BS heights and constrained BS capacities.
- The explicit expressions for the average SE are theoretically obtained based on stochastic geometry.
- We theoretically and numerically analyze the influences of the network parameters, such as the cache size of SBSs, the BS height and BS density. The results indicate that the optimal cache size, SBS density and cooperative distance threshold can be obtained such that the average SE is maximized. Moreover, the optimal cache size decreases with the expansion of the area for cooperative SBSs and the optimal cooperative distance threshold decreases with the SBS density and finally levels off. These results provide practical insights for the HetNet design and optimizations.

The remainder of this paper is organized as follows. The related works and motivation are presented in Section II. The system model and the proposed cooperative transmission strategy are presented in Section III. In Section IV, the cell load distributions of MBSs and SBSs are characterized. Then, in Section V, the SE analysis is conducted with the characterization of aggregated information and interference signal strengths. Numerical results are given in Section VI. Finally, Section VII concludes this work.

II. Related Works and Motivation

Since caching has been considered as one of the key technique in the next generation mobile networks [4], [5], cache-enabled SBSs will be widely deployed in HetNets to alleviate the load of backhaul links and to provide high data rate and low-latency services. Various studies on the analysis of cache placement and cell association in cache-enabled HetNets have been raised in literatures.

With deterministic content placement, [17] analyzed the outage probability and average delivery rate with homogeneous Poisson Point Process (HPPP) modeling of SBSs and a general popular distribution of cache files. [12] proposed a multi-cell cluster-centric cooperative transmission to improve the content availability by dividing the cache space into two parts for storing the most popular contents and less popular contents. Based on the approximated successful content delivery probability, the optimal cache space assignment was investigated. [19] studied the energy efficiency of cache-enabled cooperative small cell networks with an self-similarity based coordinated multi-point clustering strategy. To eliminate the interference generated from the neighboring BSs, [20] proposed a interference management by exploiting the content diversity. With probabilistic content placement, [9] studied the optimal caching probability with a dynamic on-off small cell network. [15] proposed a cooperative SBS transmission scheme and analyzed the successful transmission probability with stochastic geometry. The optimal content placement was further obtained with an exhaustive search algorithm. [21] also optimized the content placement probabilities with objective of cache hit probability.

In the aforementioned works, neither the influence of diverse BS heights among BSs in HetNets nor the constraint of BS capacity is considered. Modeling the cache-enabled HetNets with consideration of elevated BSs with diverse BS heights, the traditional idealized standard path loss model that does not differentiate LoS and NLoS transmissions will no longer be applicable and thus the selection of cooperative BSs should be re-designed. A more practical and accurate path loss model for the performance analysis in wireless networks is the multi-slope path loss model [22], [23]. In [22], multi-slope path loss model consisting of different path loss exponent in different distance range was studied, mainly focused on the dual-slope path loss function. Furthermore, [23] derived the coverage probability and area spectral efficiency (ASE) with general multi-slope path loss model. By incorporating dual-slope path loss model, [24] studied the downlink coverage performance of dense cellular network with elevated BSs and nearest BS association scheme.

With the consideration of constraint BS capacity, the cell load distributions of BSs is crucial in the selection of cooperative BSs, especially for low-power SBSs with low BS capacity. Thus, the impact of BS capacity should also be took into account in the design of coordination multi-point transmission. Motivated by these practical factors, we study the cooperative transmission in HetNets with cache-enabled SBSs, taking the BS height difference and BS capacity into consideration. A dual-slope path loss model is applied and an MBS-assisted cooperative transmission strategy is proposed to improve the SE by SBS offloading. Further, we theoretically obtain the average SE with stochastic geometry.

III. System model

A. Network Architecture

We consider a $(K+1)$-tier HetNet consisting of one tier elevated MBSs and K tiers elevated and cache-enabled SBSs.

The MBSs are connected to the core network through optical fiber with high capacity and provide reliable wireless coverage and connectivity, while the SBSs are cache-enabled and provide high data rate services with cached contents. The distribution of MBSs is modeled as HPPP $\Phi_0 \in \mathbb{R}^2$ with density λ_0 and the K-tier SBSs are distributed according to independent HPPPs $\Phi_k \in \mathbb{R}^2$ with density $\lambda_k, k = 1, ..., K$. The MUs are randomly distributed at the ground level and modeled as HPPP $\Phi_u \in \mathbb{R}^2$ with density λ_u. The BSs in the k-th tier are elevated at a height of H_k in meter, $k = 0, 1, ..., K$. Based on Slivnyaks theorem [25], a typical MU is located at the origin of the coordinate o.

Suppose that N_k antennas are equipped at each BS in the k-th tier. The transmission power at the BSs in the k-th tier is denoted as $P_k^{(\mathrm{TX})}$. To avoid inter-tier interference between MBSs and SBSs, orthogonal frequencies are applied at MBSs and SBSs [26]. To simultaneously serve multiple MUs without intra-cell interference, zero-forcing precoding is adopted with equal power allocation among the associated MUs in a cell. Thus, the BS capacity of the k-th tier, i.e., the maximum number of MUs that can be simultaneously served by a BS, is $M_k (\leqslant N_k)$.

B. Content Cache Model

T contents are available at the multimedia server. Denote $\mathcal{T} = [1, 2, ..., T]$ as the content library, where the contents are ranked and indexed according to the request frequency. The lower indexed content has the higher popularity. All the contents are considered to have the same size S in bits. The popularity distribution of the contents, which is also known as the content request distribution, is modeled by *Zipf* distribution [18], [27].

$$f_t = \frac{1/t^{\gamma}}{\sum_{i=1}^{T} 1/i^{\gamma}}, t \in \mathcal{T}, \tag{1}$$

where $\gamma (\geqslant 0)$ reflects the popularity distribution skewness. The cache size of the SBSs in the k-th tier is $L_k S$. The SBSs independently pro-cache the most L_k popular contents and the cached contents updates according to the varying popularity.[1] The MU randomly requests the contents according to the popularity distribution.

C. Wireless Channel Model

Signal propagation model is considered to be a composite of path loss and small-scale fading. Considering both LoS and NLoS links, a dual-slope path loss model is applied as [23], [28].

$$l_k(d) = \begin{cases} A_k^{(L)} d^{-\alpha_k^{(L)}}, \text{with probability } \Pr_k^{(L)}(d) \\ A_k^{(\mathrm{NL})} d^{-\alpha_k^{(\mathrm{NL})}}, \text{with probability } 1 - \Pr_k^{(L)}(d) \end{cases}, \tag{2}$$

where d in kilometer is the distance between the transmitter and receiver. $A_k^{(\mathrm{L})}$ and $A_k^{(\mathrm{NL})}$ are the path loss at a reference distance $d = 1(\mathrm{km})$ for the LoS and NLoS cases in the k-th tier, respectively. $\alpha_k^{(\mathrm{L})}$ and $\alpha_k^{(\mathrm{NL})}$ are the path loss exponents for the LoS and NLoS cases, respectively.

$$\Pr_k^{(L)}(d) = \begin{cases} 1 - \frac{d}{d_{k,o}}, d \in (0, d_{k,o}] \\ 0, d \in (d_{k,o}, \infty] \end{cases}, \tag{3}$$

is the probability function that a transmission link in the k-th tier has a LoS path, where $d_{k,o}$ is a parameter that determines the decreasing slope of the linear function $\Pr_k^{(\mathrm{L})}(d)$. The NLoS path loss $A_k^{(\mathrm{NL})}$ and the path loss exponent $\alpha_k^{(\mathrm{NL})}$ are respectively the increasing and decreasing functions with respect to (*w.r.t*) the BS height according to the measurements and propagation model. For example, the macro cell path loss based on modified COST (COopération européenne dans le domaine de la recherche Scientifique et Technique) 231 Hata propagation model [29] can be expressed as:

$$\begin{cases} -10\log_{10} A_0^{(\mathrm{NL})} = 46.3 + 33.9\log_{10}(f) \\ \qquad\qquad -13.82\log_{10} H_0 + 3, \\ 10\alpha_0^{(\mathrm{NL})} = 44.9 - 6.55\log_{10} H_0. \end{cases} \tag{4}$$

where f is the carrier frequency in MHz and (4) is valid when $H_0 > 35\,\mathrm{m}$. The small cell NLoS based on the COST 231 Walfish-Ikegami street canyon model [29] is given by

$$\begin{cases} -10\log_{10} A_k^{(\mathrm{NL})} = a - 18\log_{10}(1 + H_k), \\ 10\alpha_k^{(\mathrm{NL})} = 38. \end{cases} \tag{5}$$

where a is determined by the wireless environments such as the carrier frequency, the height of buildings, the building separation, the road orientation, etc. According to (4) and (5), with the rise of BS height, the path loss factors increase and the path loss exponents decrease, which results in low path loss of the signal propagation. The key notations are summarized as in Table I.

TABLE I
KEY PARAMETERS AND NOTATIONS

Symbol	Description
$\Phi_0(\lambda_0)$	HPPP model of MBSs with density λ_0
$\Phi_k(\lambda_k)$	HPPP model of SBSs with density λ_k
$\Phi_u(\lambda_u)$	HPPP model of MU with density λ_u
$P_0^{(\mathrm{TX})}$, $P_k^{(\mathrm{TX})}$	Transmission power of MBSs and SBSs
N_0, N_k	Number of antennas equipped at MBSs and SBSs in the k-th tier
M_0, M_k	BS capacity of MBSs and SBSs in the k-th tier
H_0, H_k	BS height of MBSs and SBSs in the k-th tier
$A_k^{(\mathrm{L})}$, $\alpha_k^{(\mathrm{L})}$	Path loss factor and exponent of LoS
$A_k^{(\mathrm{NL})}$, $\alpha_k^{(\mathrm{NL})}$	Path loss factor and exponent of NLoS
γ	Content popularity
T, L_k	Number of contents and cache size at SBSs in the k-th tier

D. Cooperative Transmission Strategy

An MBS-assisted cooperative transmission strategy is performed, being aware of the availability of the requested contents at the SBSs, the transmission distance between the MUs and the SBSs, and the cell load at SBSs.

To provide high data rate transmission, the cache-enabled SBSs formulate cooperative clusters to transmit the MUs' data in a user-centric manner. Fig. 1 illustrates the selection process

[1] The popularity distribution of contents is the statistical results of the content requests from the MUs. In a certain period with multiple time slots, the BSs count the request frequencies for contents and approximate the popularity of the contents within each time slot. Thus, the popularity of contents updates and changes across time slots, and the SBSs can update the cached contents according to the estimated content popularity.

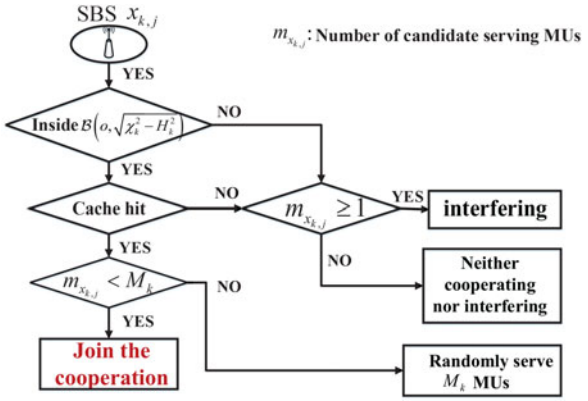

Fig. 1. Selection process of a cooperative SBS.

of a cooperative SBS. Specifically, an SBS $x_{k,j}$ in the k-th tier will join to serve the typical MU if the following events happen. E_1: the transmission distance between the SBS at $x_{k,j}$ and the typical MU is less than a predetermined distance threshold $\chi_k (\chi_k \geqslant H_k)$, i.e., the candidate cooperative SBS $x_{k,j}$ is located inside the circular area centered at the typical MU and with radius $\sqrt{\chi_k^2 - H_k^2}$ [2], i.e., $\mathcal{B}(o, \sqrt{\chi_k^2 - H_k^2})$; E_2: the requested contents are cached at the SBS $x_{k,j}$, i.e., a cache hit happens; and E_3: it surely joins to serve the typical MU if $n_{k,j} < M_k$, where $n_{k,j}$ is the number of other candidate MUs of SBS $x_{k,j}$ satisfying the conditions E_1 and E_2. Otherwise, the SBS $x_{k,j}$ randomly serves M_k candidate MUs.

With condition E_3, an SBS will serve all its candidate MUs if it is not overloaded, but will randomly choose M_k MUs otherwise. If no SBSs can provide such connections for the typical MU, i.e., the typical MU fails to be served by an SBS cluster, it will be served by its nearest MBS, to guarantee the service continuity. We consider the MBSs have sufficient capacity to support the connectivity of MUs, i.e, $\lambda_0 M_0 \gg \lambda_u$, thanks to the advanced techniques such as Massive MIMO and non-orthogonal multiple access (NOMA) [30]. When the typical MU is served by the cooperative SBS cluster, the received signal-to-interference plus noise ratio (SINR) is

$$\text{SINR}_s = \sum_{k=1}^{K} S_k \Big/ \left(\sum_{k=1}^{K} I_k + \sigma^2 \right), \tag{6}$$

where S_k and I_k are the aggregated information and interference signal strength received from the cooperative SBSs and interfering SBSs in the k-th tier, respectively.

$$S_k = \sum_{x_{k,i} \in \Phi_k \cap \mathcal{B}\left(0,\sqrt{\chi_k^2 - H_k^2}\right)} \mathbb{1}\left(E_2 \& E_3\right) \frac{P_k^{(\text{tx})}}{n_{x_{k,i}} + 1} \times l_k\left(\sqrt{|x_{k,i}|^2 + H_k^2}\right) \left\|\mathbf{h}_{x_{k,i}}\right\|_2^2, \tag{7}$$

and

$$I_k = I_{k,\text{in}} + I_{k,\text{out}}$$

[2]The radius $\sqrt{\chi_k^2 - H_k^2}$ is also referred as the radius of the serving area of an SBSs

$$= \sum_{x_{k,j} \in \Phi_k \cap \mathcal{B}\left(0,\sqrt{\chi_k^2 - H_k^2}\right)} \mathbb{1}\left(!E_2 \text{or} !E_3\right) \frac{P_k^{(\text{tx})}}{m_{x_{k,j}}} \times l_k\left(\sqrt{|x_{k,j}|^2 + H_k^2}\right) \left\|\mathbf{h}_{x_{k,j}}\right\|_2^2 + \sum_{x_{k,j} \in \Phi_k \setminus \mathcal{B}\left(0,\sqrt{\chi_k^2 - H_k^2}\right)} \mathbb{1}\left(m_{x_{k,j}} \geqslant 1\right) \frac{P_k^{(\text{tx})}}{m_{x_{k,j}}} \times l_k\left(\sqrt{|x_{k,j}|^2 + H_k^2}\right) \left\|\mathbf{h}_{x_{k,j}}\right\|_2^2 \tag{8}$$

where $!E_2$ and $!E_3$ are the opposite events of E_2 and E_3, respectively. $n_{x_{k,i}}$ and $m_{x_{k,j}}$ are the number of other candidate MUs served by the SBS $x_{k,i}$ and $x_{k,j}$, respectively. $\mathbb{1}(*)$ is an indicator function, where $\mathbb{1}(*) = \begin{cases} 1, \text{ if event} * \text{occurs} \\ 0, \text{ otherwise} \end{cases}$. $\mathbf{h}_{x_{k,i}}$ and $\mathbf{h}_{x_{k,j}}$ are the channel fading gain vectors, whose entities are identical and independent distributed (i.i.d) complex Gaussian distribution with zero mean and unit variance. If the SBS $x_{k,i}$ cooperates to serve the typical MU, $\|\mathbf{h}_{x_{k,i}}\|_2^2$ is gamma distributed $\|\mathbf{h}_{x_{k,i}}\|_2^2 \sim \Gamma(N_k - m_{x_{k,i}}, 1)$ [31]. Otherwise, if the SBS $x_{k,j}$ is an interfering SBS, $\|\mathbf{h}_{x_{k,j}}\|_2^2$ is gamma distributed with parameters $m_{x_{k,j}}$ and 1, i.e., $\|\mathbf{h}_{x_{k,j}}\|_2^2 \sim \Gamma(m_{x_{k,j}}, 1)$ [32].

Denote $x_{0,0}$ as the nearest MBS to the typical MU, and define $r_0 \triangleq |x_{0,0}|$. If the typical UE fails to be served by cooperative SBS cluster, it will be served by $x_{0,0}$ and the received SINR is

$$\text{SINR}_m = \mathbb{1}\left(\text{empty cooperative cluster}\right) \times \frac{\frac{P_0^{(\text{TX})}}{n_{x_{0,0}}+1} l_0\left(\sqrt{|x_{0,0}|^2 + H_0^2}\right) \|\mathbf{h}_0\|_2^2}{I_0 + \sigma^2}, n_{x_{0,0}} < M_0, \tag{9}$$

where

$$I_0 = \sum_{x_{0,j} \in \Phi_0 \setminus x_{0,0}} \mathbb{1}\left(m_{x_{0,j}} \geqslant 1\right) \frac{P_0^{(\text{TX})}}{m_{x_{0,j}}} l_0\left(\sqrt{|x_{0,j}|^2 + H_0^2}\right) \|\mathbf{h}_j\|_2^2 \tag{10}$$

is the aggregated interference strength. $n_{x_{0,0}}$ and $m_{x_{0,j}}$ are the number of other candidate MUs with the MBS $x_{0,0}$ and $x_{0,j}$, respectively. Note that the channel fading $\|\mathbf{h}_0\|_2^2$ and $\|\mathbf{h}_j\|_2^2$ are gamma distributed, i.e., $\|\mathbf{h}_0\|_2^2 \sim \Gamma(N_0 - m_{x_{0,0}}, 1)$ and $\|\mathbf{h}_j\|_2^2 \sim \Gamma(m_{x_{0,j}}, 1)$.

From the expressions (6)–(9), the distributions of cell load have great influence on the determination of cooperative SBSs as well as the received signal strength. To analyze the statistics of the received SINR, we have to obtain the cell load distributions of MBSs and SBSs.

IV. Cell Load Distribution

A. Distribution of SBS Load

Define the cell load as the number of MUs simultaneously served by an elevated BS. For the SBSs in the k-th tier, the probability that an SBS has stored the requested contents is $\eta_k = \sum_{t=1}^{L_k} f_t$. With the cooperative transmission strategy, the event that $m_k (< M_k)$ MUs are served by an SBS located at

$x_{k,i}$ is equivalent to the event that more than m_k MUs located inside $\mathcal{B}(x_{k,i}, \sqrt{\chi_k^2 - H_k^2})$ while only m_k cache hits happen. Mathematically, the probability that $m_k (< M_k)$ MUs are served with an SBS located at $x_{k,i}$ is

$$\begin{aligned}\rho_k(m_k) &\overset{(a)}{=} \sum_{n=m_k}^{\infty} \frac{\left(\pi\left(\chi_k^2 - H_k^2\right)\lambda_u\right)^n \exp\left(-\pi\left(\chi_k^2 - H_k^2\right)\lambda_u\right)}{n!} \\ &\quad \times \frac{n!}{m_k!\,(n-m_k)!}(\eta_k)^{m_k}(1-\eta_k)^{n-m_k} \\ &\overset{(b)}{=} \frac{\left(\pi\left(\chi_k^2 - H_k^2\right)\eta_k\lambda_u\right)^{m_k}\exp\left(-\pi\left(\chi_k^2 - H_k^2\right)\eta_k\lambda_u\right)}{m_k!},\end{aligned} \tag{11}$$

where (a) holds due to the PPP distribution of MUs and the binomial distribution of cache hits among n UEs; and (b) follows the Taylor Expansion. Since the event of full-loaded at an SBSs is equivalent to the event that more than M_k candidate serving MUs request for the connection, the probability of $m_k = M_k$ is

$$\rho_k(M_k) = \sum_{m=M_k}^{\infty} p_k(m), \tag{12}$$

where $p_k(m) = \frac{(\pi(\chi_k^2 - H_k^2)\eta_k\lambda_u)^m \exp(-\pi(\chi_k^2 - H_k^2)\eta_k\lambda_u)}{m!}$.

Define the offloading probability as the probability that an MU is offloaded from MBSs to SBSs. Based on the cell load distribution of SBSs, we have the offloading probability as the following proposition.

Proposition 1: In the HetNets with MBS-assisted and content-aware cooperative transmission strategy, the offloading probability is $1 - \nu$, where $\nu = \prod_{k=1}^{K} \nu_k$ with

$$\nu_k = \exp\left(-\pi\left(\chi_k^2 - H_k^2\right)\phi_k\lambda_k\right). \tag{13}$$

Proof: For the SBSs in the k-th tier, denote ϕ_k as the probability that a random SBS located inside $\mathcal{B}(o, \sqrt{\chi_k^2 - H_k^2})$ joins to serve the typical MU. With the cooperative transmission scheme, ϕ_k is given by:

$$\phi_k = \eta_k\left(\sum_{n=0}^{M_k-1} p_k(n+1) + \sum_{n=M_k}^{\infty} p_k(n+1)\frac{M_k}{n+1}\right), \tag{14}$$

where n is the number of other candidate MUs of the SBS. By thinning property of PPP, the SBSs that locate inside $\mathcal{B}(o, \sqrt{\chi_k^2 - H_k^2})$ and can provide connections for the typical MU form a PPP with density $\phi_k\lambda_k$. Thus, the probability that zero SBSs in the k-th tier can provide services for the typical MU is ν_k, and the probability that the typical MU is served by its nearest MBS is $\nu = \prod_{k=1}^{K} \nu_k$. ■

B. Distribution of MBS Load

With Proposition 1, all the MUs served by the MBSs form a thinning PPP with density $\lambda_u^{'} = \nu\lambda_u$. Since the MUs are associated with MBSs in a nearest way, the resulting network topology of macrocell network is Poisson Voronoi (PV) tessellation. The probability density function (*pdf*) of the cell size with the PV tessellation is accurately approximated as [33], [34]:

$$f(A) = \frac{(3.5\lambda_0)^{3.5}}{\Gamma(3.5)} A^{2.5}\exp(-3.5\lambda_0 A). \tag{15}$$

Thus, the cell load distribution of MBSs when $m_0 < M_0$ is

$$\begin{aligned}\rho_0(m_0) &= \int_0^{\infty} \frac{\left(\lambda_u^{'}A\right)^{m_0} e^{-\lambda_u^{'}A}}{m_0!} f(A)\,\mathrm{d}A \\ &= \frac{3.5^{3.5}\Gamma(m_0+3.5)}{m_0!\Gamma(3.5)} \frac{\left(\lambda_u^{'}/\lambda_0\right)^{m_0}}{\left(3.5+\lambda_u^{'}/\lambda_0\right)^{m_0+3.5}},\end{aligned} \tag{16}$$

and the probability of $m_0 = M_0$ is

$$\rho_0(M_0) = 1 - \sum_{m_0=0}^{M_0-1} \rho_0(m_0). \tag{17}$$

As mentioned before, the MBS capacity is large enough to provide the basic connectivity. Thus, the probability $\sum_{m_0=0}^{M_0-1}\rho_0(m_0)$ approximately equals to 1, i.e., $\sum_{m_0=0}^{M_0-1}\rho_0(m_0) \approx 1$ and $\rho_0(M_0) \approx 0$.

Remark: According to (11), the density of MUs, the height of SBSs, the cooperative distance threshold, and the cache size of SBSs have direct impacts on the cell load distribution of SBSs, which further influence the offloading probability and cell load distribution of MBSs as indicated in (13), (14) and (16). Detailed, when the SBS height is equal to the cooperative distance threshold, the SBSs will not join to serve MUs and the MUs will be served by the MBSs with nearest-BS association. With denser SBSs, lower SBS height or larger cooperative distance threshold and cache size, more MUs will be offloaded to the SBSs. However, the SBSs tend to be heavy-loaded or even full-loaded with the increase in the SBS density, the cooperative distance threshold and the cache size, or with the decrease of the SBS height. In such a scenario, the received SINR at the MUs served by cooperative SBS cluster will definitely be reduced.

V. Spectral Efficiency Analysis

To investigate the statistics of the received SINR at the typical MU, we theoretically analyze the average SE in this section. Define

$$\begin{aligned}S_0 &= \mathbb{1}(\text{empty cooperative cluster}) \\ &\quad \times \frac{P_0^{(\mathrm{TX})}}{m_{x_{0,0}}+1} l_0\left(\sqrt{|x_{0,0}|^2 + H_0^2}\right)\|\mathbf{h}_0\|_2^2,\end{aligned} \tag{18}$$

the average SE when the typical MU is served by the nearest MBS is

$$\begin{aligned}\mathcal{R}_m &= \mathbb{E}\left[\ln\left(1+\mathrm{SINR}_m\right)\right] \\ &\overset{(d)}{=} \mathbb{E}_{|x_{0,0}|}\left[\int_0^{\infty} \frac{\mathcal{L}_{I_0}(t|\,|x_{0,0}|)\left(1-\mathcal{L}_{S_0}(t|\,|x_{0,0}|)\right)}{t} e^{-\sigma^2 t}\mathrm{d}t\right]\end{aligned} \tag{19}$$

in nats/s/Hz. (d) is obtained with the results in [35]. $\mathcal{L}_X(t)$ is the Laplace function of X. Similarly, the average SE when the

typical MU is served by the cooperative SBS cluster is

$$\mathcal{R}_s = \mathbb{E}\left[\ln\left(1+\text{SINR}_s\right)\right] = \int_0^\infty \frac{\prod_{k=1}^{K}\mathcal{L}_{I_k}(t)\left(1-\prod_{k=1}^{K}\mathcal{L}_{S_k}(t)\right)}{t} e^{-\sigma^2 t}\mathrm{d}t, \quad (20)$$

in nats/s/Hz. We defined the average user SE as the sum SE that can be achieved at the typical MU, i.e.,

$$\mathcal{R} = \mathcal{R}_s + \mathcal{R}_m. \quad (21)$$

A. Average SE With MBS Association

1) Statistics of $|x_{0,0}|$: With the PPP modeling of MBSs, the *pdf* of r_0 is $f_{r_0}(r) = 2\pi\lambda_0 r e^{-\pi\lambda_0 r^2}$. According to the path loss model (2), the distribution of $|x_{0,0}|$ is different across area. When $\sqrt{r_0^2+H_0^2} \leqslant d_{0,o}$, the signals go NLoS and LoS with probability $1-\Pr_0^L(\sqrt{r_0^2+H_0^2})$ and $\Pr_0^{(\mathrm{L})}(\sqrt{r_0^2+H_0^2})$, respectively. Denote $X_0^{(\mathrm{NL})}$ and $X_0^{(\mathrm{L})}$ as the distance between the typical MU and its serving MBS with NLOS and LOS, respectively. Then, the event $X_0^{(\mathrm{NL})} > x$ is the event of $r_0 > x$ and the nearest MBS is with NLOS. As a result, the cumulative distribution function (*cdf*) of $X_0^{(\mathrm{NL})}$ is

$$\begin{aligned} F_{X_0^{(\mathrm{NL})}}(x) &= 1-\Pr\{x_0 > x\} \\ &= 1-\Pr\{r_0 > x, \text{nearest MBS with NLOS}\} \\ &= 1-\int_x^\infty \left(1-\Pr_k^{(\mathrm{L})}\left(\sqrt{r^2+H_0^2}\right)\right) 2\pi\lambda_0 r e^{-\pi\lambda_0 r^2}\mathrm{d}r \\ &= 1-\int_x^\infty \frac{\sqrt{r^2+H_0^2}}{d_{0,o}} 2\pi\lambda_0 r e^{-\pi\lambda_0 r^2}\mathrm{d}r. \end{aligned} \quad (22)$$

Taking the derivative of $F_{X_0^{(\mathrm{NL})}}(x)$ *w.r.t* x, we have the *pdf* of $X_0^{(\mathrm{NL})}$ as:

$$f_{X_0^{(\mathrm{NL})}}(x) = \frac{\sqrt{x^2+H_0^2}}{d_{0,o}} 2\pi\lambda_0 x e^{-\pi\lambda_0 x^2}. \quad (23)$$

Similarly, when the signals are with LoS, the *pdf* of $X_0^{(\mathrm{L})}$ is

$$f_{X_0^{(L)}}(x) = \left(1-\frac{\sqrt{x^2+H_0^2}}{d_{0,o}}\right) 2\pi\lambda_0 x e^{-\pi\lambda_0 x^2}. \quad (24)$$

When $\sqrt{r_0^2+H_0^2} > d_{0,o}$, the signals are with NLoS with probability 1. Denote X_0 as the distance between the typical MU and its serving MBS, the *pdf* of X_0 is

$$f_{X_0}(x) = 2\pi\lambda_0 x \exp\left(-\pi\lambda_0 x^2\right). \quad (25)$$

It can be seen from (23)–(25) that the probability of NLoS increases with the rise of BS height.

2) Laplace Functions of S_0 and I_0: With the definition of S_0, the Laplace function of S_0 conditioned on r_0 is

$$\begin{aligned} \mathcal{L}_{S_0}(t|r_0) &= \mathbb{E}_{S_0}\left(e^{-tS_0}\right) \\ &\overset{(d)}{\approx} 1-\nu+\nu\sum_{n_0=0}^{M_0-2}\rho_0(n_0+1) \\ &\quad\times\int_0^\infty e^{-t\frac{P_0^{(\mathrm{TX})}}{n_0+1}l_0\left(\sqrt{r_0^2+H_0^2}\right)h}\frac{h^{N_0-n_0-1}}{\Gamma(N_0-n_0)}e^{-h}dh \\ &= 1-\nu+\nu\sum_{n_0=0}^{M_0-2}\frac{\rho_0(n_0+1)}{\left(1+\frac{tP_0^{(\mathrm{TX})}}{n_0+1}l_0\left(\sqrt{r_0^2+H_0^2}\right)\right)^{(N_0-n_0)}}, \end{aligned} \quad (26)$$

where (d) follows $\|\mathbf{h}_0\|_2^2 \sim \Gamma(N_0-m_{x_{0,0}},1)$ and ignores the item $\rho_0(M_0)$. With NLoS and LoS for the path loss, $\mathcal{L}_{S_0}(t|r_0)$ can be re-written as:

$$\begin{aligned} \mathcal{L}_{S_0}^{(*)}(t|r_0) &= 1-\nu+\nu \\ &\quad\times\sum_{n_0=0}^{M_0-2}\rho_0(n_0+1)\left(1+\frac{tP_0^{(\mathrm{TX})}A_0^{(*)}}{(n_0+1)\left(r_0^2+H_0^2\right)^{\frac{\alpha_0^{(*)}}{2}}}\right)^{(n_0-N_0)} \end{aligned} \quad (27)$$

where (*) is (NL) for NLoS and (L) for LoS.

The statistics of I_0 are analyzed with two cases: $0 < r_0 \leqslant \sqrt{(d_{0,o})^2-H_0^2}$ and $r_0 > \sqrt{(d_{0,o})^2-H_0^2}$.

Lemma 1: • When $0 < r_0 \leqslant \sqrt{(d_{0,o})^2-H_0^2}$, the Laplace function of I_0 conditioned on r_0 is

$$\mathcal{L}_{I_{0,1}}(t|r_0) = \exp\left(-\pi\lambda_0\sum_{m=1}^{M_0}\rho_0(m)\,\mu_{0,1}(m,t,r_0)\right), \quad (28)$$

where

$$\begin{aligned} \mu_{0,1}(m,t,r_0) &= \mathcal{Z}\left(\alpha_0^{(L)},m,2,m,P_0^{(\mathrm{TX})}A_0^{(L)},d_{0,o}\right) \\ &\quad-\mathcal{Z}\left(\alpha_0^{(L)},m,2,m,P_0^{(\mathrm{TX})}A_0^{(L)},\sqrt{r_0^2+H_0^2}\right) \\ &\quad+\frac{2}{3}\begin{pmatrix}\mathcal{Z}\left(\alpha_0^{(\mathrm{NL})},m,3,m,P_0^{(\mathrm{TX})}A_0^{(\mathrm{NL})},d_{0,o}\right)\\ -\mathcal{Z}\left(\alpha_0^{(L)},m,3,m,P_0^{(\mathrm{tx})}A_0^{(L)},d_{0,o}\right)\end{pmatrix} \\ &\quad-\frac{2\sqrt{r_0^2+H_0^2}}{3d_{0,o}} \\ &\quad\times\begin{pmatrix}\mathcal{Z}\left(\alpha_0^{(\mathrm{NL})},m,3,m,P_0^{(\mathrm{TX})}A_0^{(\mathrm{NL})},\sqrt{r_0^2+H_0^2}\right)\\ -\mathcal{Z}\left(\alpha_0^{(L)},m,3,m,P_0^{(\mathrm{TX})}A_0^{(L)},\sqrt{r_0^2+H_0^2}\right)\end{pmatrix} \\ &\quad-\mathcal{Z}\left(\alpha_0^{(\mathrm{NL})},m,2,m,P_0^{(\mathrm{TX})}A_0^{(\mathrm{NL})},d_{0,o}\right), \end{aligned} \quad (29)$$

$$\mathcal{R}_m \approx \int_0^{\sqrt{(d_{0,o})^2-H_0^2}} \int_0^{\infty} \frac{e^{-\pi\lambda_0 \sum_{m=1}^{M_0} \rho_0(m)\mu_{0,1}(m,t,x)} e^{-\sigma^2 t}}{t} \left(1-\mathcal{L}_{S_0}^{(NL)}(t|x)\right) \mathrm{d}t f_{X_0^{(\mathrm{NL})}}(x)\,\mathrm{d}x + \int_0^{\sqrt{(d_{0,o})^2-H_0^2}} \int_0^{\infty} \frac{e^{-\pi\lambda_0 \sum_{m=1}^{M_0} \rho_0(m)\mu_{0,1}(m,t,x)} e^{-\sigma^2 t}}{t} \left(1-\mathcal{L}_{S_0}^{(L)}(t|x)\right) \mathrm{d}t f_{X_0^{(L)}}(x)\,\mathrm{d}x + \int_{\sqrt{(d_{0,o})^2-H_0^2}}^{\infty} \int_0^{\infty} \frac{e^{-\pi\lambda_0 \sum_{m=1}^{M_0} \rho_0(m)\mu_{0,2}(m,t,x)} e^{-\sigma^2 t}}{t} \left(1-\mathcal{L}_{S_0}^{(NL)}(t|x)\right) \mathrm{d}t f_{X_0}(x)\mathrm{d}x \tag{33}$$

with

$$\mathcal{Z}(\alpha, n_1, n_2, n_3, c, x) = x^2 \left(1 - {}_2F_1\left(n_1, -\frac{n_2}{\alpha}; 1-\frac{n_2}{\alpha}; -\frac{tc}{n_3 x^{\alpha}}\right)\right). \tag{30}$$

${}_2F_1(a,b;c;z)$ is the Hypergeometric function.

- When $r_0 > \sqrt{(d_{0,o})^2 - H_0^2}$, the Laplace function of I_0 is

$$\mathcal{L}_{I_{0,2}}(t|r_0) = \exp\left(\pi\lambda_0 \sum_{m=1}^{M_0} \rho_0(m)\,\mu_{0,2}(m,t,r_0)\right), \tag{31}$$

where

$$\mu_{0,2}(m,t,r_0) = \mathcal{Z}\left(\alpha_0^{(\mathrm{NL})}, m, 2, m, P_0^{(\mathrm{TX})} A_0^{(\mathrm{NL})}, \sqrt{r_0^2+H_0^2}\right). \tag{32}$$

Proof: Please refer to Appendix A. ■

Combining (27) and (28) with (19), the average SE $\mathcal{R}_m$ can be obtained as the following theorem.

Theorem 1: In cache-enabled HetNets with the MBS-assisted and content-aware cooperative transmission strategy, the average SE when an MU is served by its nearest MBS is given in (33), shown at the top of the page.

Proof: The result can be obtained by substituting (23)–(25) and (27) into (19). ■

According to (27)–(33), when the distance between the nearest MBS and the typical UE is less than $\sqrt{(d_{0,o})^2 - H_0^2}$, the Laplace function $\mathcal{L}_{S_0}^{(\mathrm{NL})}(t|X_0^{(\mathrm{NL})})$ and the probability for having NLoS increase with the MBS height, which results in the decrease of the first two items in (33). Similarly, when $r_0 > \sqrt{(d_{0,o})^2 - H_0^2}$, the third item decreases with the increasing MBS height. Overall, when the MUs are served by the MBSs, the average SE $\mathcal{R}_m$ decreases with rise of the MBS height. In addition, we can see from (16) that with increasing MBS density, the cell load at MBSs is relaxed and finally approximated to zero, i.e., $\lim_{\lambda_0\to\infty} \rho_0(0) \approx 1$. Moreover, the distance between the typical MU and its nearest MBS decreases and finally level off to 0 with the increase of the MBS density. In such a scenario, the BS height is the key factor that determines the SE performance $\mathcal{R}_m$.

B. Average SE With Cooperative SBS Cluster Association

Similar to the analysis of $\mathcal{L}_{I_0}(t)$, the Laplace functions $\mathcal{L}_{S_k}(t)$ and $\mathcal{L}_{I_k}(t)$ in (20) are analyzed with the cases $0 < \chi_k \leqslant d_{k,o}$ and $\chi_k > d_{k,o}$.

Lemma 2: The Laplace function of S_k is

$$\mathcal{L}_{S_k}(t) = \exp\left(-\pi\lambda_k\eta_k \sum_{n_k=0}^{M_k-1} p_k(n_k+1)\,\varpi_k(N_k-n_k, n_k+1)\right) \times \exp\left(-\pi\lambda_k\eta_k\varpi_k(N_k-M_k+1, M_k) \sum_{n_k=M_k}^{\infty} \frac{p_k(n_k+1)M_k}{n_k+1}\right) \tag{34}$$

- When $0 < \chi_k \leqslant d_{k,o}$, $\varpi_k(m,n)$ is re-expressed as:

$$\begin{aligned}\varpi_{k,1}(m,n) &= \mathcal{Z}\left(\alpha_k^{(L)}, m, 2, n, P_k^{(\mathrm{TX})} A_k^{(L)}, \chi_k\right) - \mathcal{Z}\left(\alpha_k^{(L)}, m, 2, n, P_k^{(\mathrm{TX})} A_k^{(L)}, H_k\right) \\ &+ \frac{2\chi_k}{3d_{k,o}} \begin{pmatrix} \mathcal{Z}\left(\alpha_k^{(\mathrm{NL})}, m, 3, n, P_k^{(\mathrm{TX})} A_k^{(\mathrm{NL})}, \chi_k\right) \\ -\mathcal{Z}\left(\alpha_k^{(L)}, m, 3, n, P_k^{(\mathrm{TX})} A_k^{(L)}, \chi_k\right) \end{pmatrix} \\ &- \frac{2H_k}{3d_{k,o}} \begin{pmatrix} \mathcal{Z}\left(\alpha_k^{(\mathrm{NL})}, m, 3, n, P_k^{(\mathrm{TX})} A_k^{(\mathrm{NL})}, H_k\right) \\ -\mathcal{Z}\left(\alpha_k^{(L)}, m, 3, n, P_k^{(\mathrm{TX})} A_k^{(L)}, H_k\right) \end{pmatrix}\end{aligned} \tag{35}$$

- When $\chi_k > d_{k,o}$, $\varpi_k(m,n)$ is re-expressed as:

$$\begin{aligned}\varpi_{k,2}(m,n) &= \mathcal{Z}\left(\alpha_k^{(L)}, m, 2, n, P_k^{(\mathrm{TX})} A_k^{(L)}, d_{k,o}\right) - \mathcal{Z}\left(\alpha_k^{(L)}, m, 2, n, P_k^{(\mathrm{TX})} A_k^{(L)}, H_k\right) \\ &+ \mathcal{Z}\left(\alpha_k^{(\mathrm{NL})}, m, 2, n, P_k^{(\mathrm{TX})} A_k^{(\mathrm{NL})}, \chi_k\right) - \mathcal{Z}\left(\alpha_k^{(\mathrm{NL})}, m, 2, n, P_k^{(\mathrm{TX})} A_k^{(\mathrm{NL})}, d_{k,o}\right) \\ &+ \frac{2}{3} \begin{pmatrix} \mathcal{Z}\left(\alpha_k^{(\mathrm{NL})}, m, 3, n, P_k^{(\mathrm{TX})} A_k^{(\mathrm{NL})}, d_{k,o}\right) \\ -\mathcal{Z}\left(\alpha_k^{(L)}, m, 3, n, P_k^{(\mathrm{TX})} A_k^{(L)}, d_{k,o}\right) \end{pmatrix} \\ &- \frac{2H_k}{3d_{k,o}} \begin{pmatrix} \mathcal{Z}\left(\alpha_k^{(\mathrm{NL})}, m, 3, n, P_k^{(\mathrm{TX})} A_k^{(\mathrm{NL})}, H_k\right) \\ -\mathcal{Z}\left(\alpha_k^{(L)}, m, 3, n, P_k^{(\mathrm{TX})} A_k^{(L)}, H_k\right) \end{pmatrix}\end{aligned} \tag{36}$$

when $H_k < d_{k,o}$. Otherwise, when $H_k > d_{k,o}$, $\varpi_k(m,n)$ is re-expressed as:

$$\varpi_{k,3}(m,n) = \mathcal{Z}\left(\alpha_k^{(\mathrm{NL})}, m, 2, n, P_k^{(\mathrm{TX})} A_k^{(\mathrm{NL})}, \chi_k\right) - \mathcal{Z}\left(\alpha_k^{(\mathrm{NL})}, m, 2, n, P_k^{(\mathrm{TX})} A_k^{(\mathrm{NL})}, H_k\right) \tag{37}$$

Proof: Please refer to Appendix B. ■

As provided in (8), the interference generated by SBSs in the k-th tier includes the interference caused by the SBSs inside $\mathcal{B}(o,\chi_k)$ and outside $\mathcal{B}(o,\chi_k)$. According to the definition of Laplace transform, $\mathcal{L}_{I_k}(t)$ can be re-written as:

$$\mathcal{L}_{I_k}(t)=\mathcal{L}_{I_{k,\text{in}}}(t)\,\mathcal{L}_{I_{k,\text{out}}}(t) \tag{38}$$

Lemma 3: The Laplace function of $I_{k,\text{in}}$ is

$$\mathcal{L}_{I_{k,\text{in}}}(t)=\exp\left(-\pi\lambda_k(1-\eta_k)\sum_{m_k=1}^{M_k-1}\rho_k(m_k+1)\,\mu_{k,\text{in}}(m_k)\right)\times\exp\left(-\pi\lambda_k\mu_{k,\text{in}}(M_k)\sum_{m_k=M_k}^{\infty}p_k(m_k+1)\left(1-\frac{\eta_k M_k}{m_k+1}\right)\right), \tag{39}$$

where

$$\mu_{k,\text{in}}(m_k)=\begin{cases}\varpi_{k,1}(m_k,m_k),0<\chi_k\leqslant d_{k,o}\\ \varpi_{k,2}(m_k,m_k),\chi_k>d_{k,o}>H_k\\ \varpi_{k,3}(m_k,m_k),\chi_k>d_{k,o},H_k\geqslant d_{k,o}.\end{cases} \tag{40}$$

The Laplace function of $I_{k,\text{out}}$ is

$$\mathcal{L}_{I_{k,\text{out}}}(t)=\exp\left(-\pi\lambda_k\sum_{m_k=1}^{M_k}\rho_k(m_k)\,\mu_{k,\text{out}}(m_k)\right), \tag{41}$$

• When $0<\chi_k\leqslant d_{k,o}$, $\mu_{k,\text{out}}(m_k)$ is re-expressed as:

$$\begin{aligned}\mu_{k,\text{out},1}(m_k)=&\,\mathcal{Z}\left(\alpha_k^{(L)},m_k,2,m_k,P_k^{(\text{TX})}A_k^{(L)},d_{k,o}\right)\\&-\mathcal{Z}\left(\alpha_k^{(L)},m_k,2,m_k,P_k^{(\text{TX})}A_k^{(L)},\chi_k\right)\\&+\frac{2}{3}\begin{pmatrix}\mathcal{Z}\left(\alpha_k^{(\text{NL})},m_k,3,m_k,P_k^{(\text{TX})}A_k^{(\text{NL})},d_{k,o}\right)\\-\mathcal{Z}\left(\alpha_k^{(L)},m_k,3,m_k,P_k^{(\text{TX})}A_k^{(L)},d_{k,o}\right)\end{pmatrix}\\&-\frac{2\chi_k}{3d_{k,o}}\begin{pmatrix}\mathcal{Z}\left(\alpha_k^{(\text{NL})},m_k,3,m_k,P_k^{(\text{TX})}A_k^{(\text{NL})},\chi_k\right)\\-\mathcal{Z}\left(\alpha_k^{(L)},m_k,3,m_k,P_k^{(\text{TX})}A_k^{(L)},\chi_k\right)\end{pmatrix}\\&-\mathcal{Z}\left(\alpha_k^{(\text{NL})},m_k,2,m_k,P_k^{(\text{TX})}A_k^{(\text{NL})},d_{k,o}\right)\end{aligned} \tag{42}$$

• When $\chi_k>d_{k,o}$, $\mu_{k,\text{out}}(m_k)$ is re-expressed as:

$$\mu_{k,\text{out},2}(m_k)=\mathcal{Z}\left(\alpha_k^{(\text{NL})},m_k,2,m_k,P_k^{(\text{TX})}A_k^{(\text{NL})},\chi_k\right). \tag{43}$$

Proof: Please refer to Appendix C. ■

Remarks: According to Lemmas 1–3, the BS height H_k, the cooperative distance threshold χ_k, the cache size of SBSs L_k and the SBS density λ_k have great influence on the statistics of the S_k and I_k. For fixed H_k with small χ_k or fixed χ_k with large H_k, the area for candidate cooperative SBSs and the number of candidate SBSs are very small. With increasing χ_k or with decreasing H_k, the area for candidate cooperative SBSs becomes wider and the number of candidate SBSs increases. However, according to the cell load distribution (11), the SBSs tend to be heavy-loaded and thus the probability that an SBS can join the cooperative cluster decreases. In conclusion, there is a tradeoff between the number for candidate SBSs and the probability for joining the cooperation with the varying radius of area for the candidate cooperative SBSs, i.e., $\sqrt{\chi_k^2-H_k^2}$. Moreover, we can see from (34) and (39) that there is a tradeoff between the cooperating probability ϕ_k and the interfering probability $(1-\eta_k)\sum_{m_k=1}^{M_k-1}\rho_k(m_k)+\sum_{m_k=M_k}^{\infty}p_k(m_k)(1-\frac{\eta_k M_k}{m_k+1})$ with the varying of the cache hit probability and the cell load at SBSs. Combining the cell load distribution (11), it can be seen that there is a tradeoff between S_k and I_k with the varying of the cache size and the radius $\sqrt{\chi_k^2-H_k^2}$.

Combining $\mathcal{L}_{I_k}(t)$, $\mathcal{L}_{S_k}(t)$ with (20), the average SE with cooperative SBS cluster serving is obtained.

Theorem 2: In cache-enabled HetNets with the MBS-assisted and content-aware cooperative transmission strategy, the average SE when the typical MU is served by cooperative SBS cluster is given as:

$$\mathcal{R}_s=\int_0^{\infty}\prod_{k=1}^{K}e^{-\pi\lambda_k\psi_k(t)}\left(1-\prod_{k=1}^{K}e^{-\pi\lambda_k\zeta_k(t)}\right)\frac{e^{-\sigma^2 t}}{t}dt \tag{44}$$

where

$$\begin{aligned}\psi_k(t)=&\,(1-\eta_k)\sum_{m_k=1}^{M_k-1}\rho_k(m_k+1)\,\mu_{k,\text{in}}(m_k)\\&+\sum_{m_k=M_k}^{\infty}p_k(m_k+1)\left(1-\frac{\eta_k M_k}{m_k+1}\right)\mu_{k,\text{in}}(M_k)\\&+\sum_{m_k=1}^{M_k}\rho_k(m_k)\,\mu_{k,\text{out}}(m_k).\end{aligned} \tag{45}$$

$\mu_{k,\text{in}}(m_k)$ and $\mu_{k,\text{out}}(m_k)$ can be respectively replaced by expressions (40), (42) and (43) depending on the cooperative distance threshold χ_k. Finally, $\zeta_k(t)$ is defined as:

$$\begin{aligned}\zeta_k(t)=&\,\eta_k\sum_{n_k=0}^{M_k-1}p_k(n_k+1)\,\varpi_k(N_k-n_k,n_k+1)\\&+\eta_k\sum_{n_k=M_k}^{\infty}\frac{p_k(n_k+1)M_k}{n_k+1}\varpi_k(N_k-M_k+1,M_k).\end{aligned} \tag{46}$$

Comparing the results with existing literatures [23], [36]–[38], it is found that the BS height, the cache size of SBSs and the cooperative distance threshold are the key parameters that influence the statistics of the aggregated information and interference signal strength, which further influence the SE of the network. In addition, according to (44), there is a tradeoff between $\mathcal{L}_{S_k}(t)$ and $\mathcal{L}_{I_k}(t)$ with the varying SBS density, i.e., λ_k. As proved in [39], there exists an optimal SBS density λ_k such that the average SE $\mathcal{R}_s$ can be maximized.

VI. Numerical Results

In this section, we numerically evaluate the average SE in a two-tier HetNet composed of MBSs and one tier cache-enabled SBSs. Simulation results are also presented with Monte Carlo methods in a circular area with radius 5 km. All the results are based on 10 MHz bandwidth system with 2 GHz carrier. The LoS exponents for macrocell are $\alpha_0^{(\text{L})}=2.42$, $A_0^{(\text{L})}=10^{-10.34}$ [40]. The NLoS for the macrocell is obtained according to Hata

TABLE II
SYSTEM PARAMETERS

Parameter	Value
$\lambda_0, \lambda_1, \lambda_u$	$\frac{1}{\pi 500^2}, \frac{3}{\pi 500^2}, \frac{5}{\pi 500^2}$
M_0, N_0, H_0	32, 32 , 150 m
M_1, N_1, H_1	4, 4 , 50 m
$P_0^{(\mathrm{TX})}, P_1^{(\mathrm{TX})}$	37 dBm, 30 dBm
d_0, d_1	0.3 km, 0.1 km
$\alpha_0^{(\mathrm{L})}, A_0^{(\mathrm{L})}$	2.42, $10^{-10.34}$
$\alpha_1^{(\mathrm{L})}, A_1^{(\mathrm{L})}$	2.09, $10^{-10.38}$
T, L_1, γ_1	200, 50, 0.8
σ^2 (10 MHz)	-104 dBm

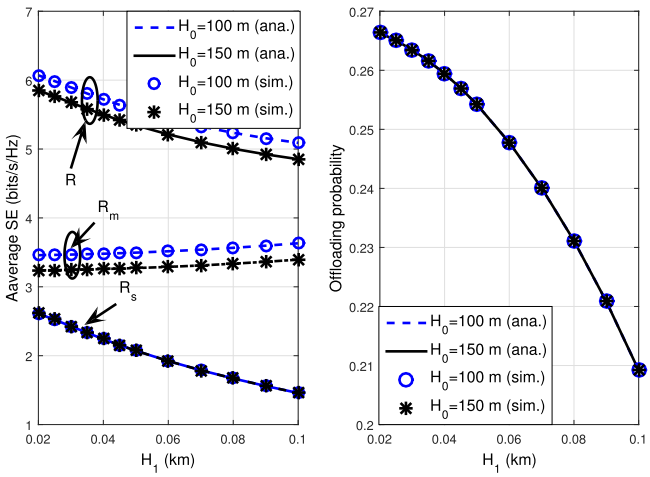

Fig. 2. Average SE and offloading probability w.r.t H_1. $\chi_1 = 0.2$ km.

model (47) with 2 GHz carrier and $H_0 > 35$ m.

$$\begin{cases} -10\log_{10}A_0^{(\mathrm{NL})} = 161.2 - 13.82\log_{10}H_0 \\ 10\alpha_0^{(\mathrm{NL})} = 44.9 - 6.55\log_{10}H_0, \end{cases} \tag{47}$$

The NLoS for small cell is obtained according to Walfish-Ikegami street canyon model with $H_1 > 20$ m.

$$\begin{cases} -10\log_{10}A_1^{(\mathrm{NL})} = 160.4 - 18\log_{10}(1 + H_1) \\ 10\alpha_1^{(\mathrm{NL})} = 38. \end{cases} \tag{48}$$

The LOS for the macrocell and small cell are adopted as that in [40]. The detailed system parameters are given in Table II unless otherwise specified.

The impact of the BS height is presented in Fig. 2, It shows that the simulations match well with the analytical results, which verifies the accuracy of the theoretical analysis. Moreover, it can be seen that the average SE R decreases with the BS height. Specially, the offloading probability also decreases with increasing SBS height H_1 while the MBS height has no impact on the offloading probability. In addition, with the rise of SBS height, the average SE R_s provided by SBSs decreases while the average SE R_m provided by MBSs increases. The decrease of R_s is due to i) the reduce of the offloading probability, which makes more MUs associated with MBSs, ii) the shrink of the area for candidate cooperative SBSs, and iii) the COST 231 Hata model for channel fading. The increase of R_m is because

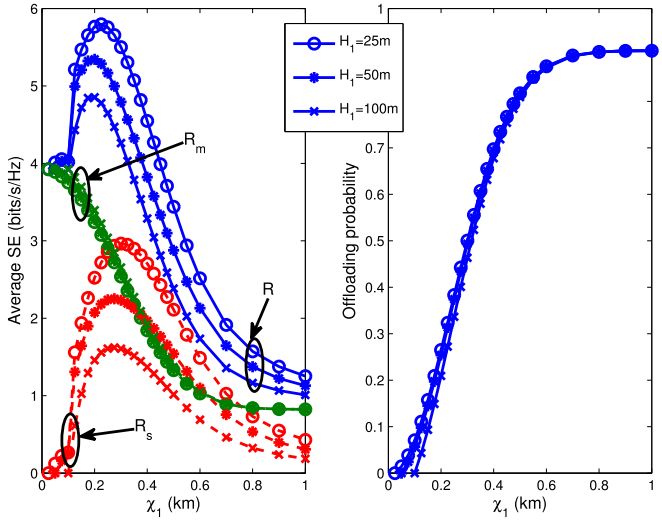

Fig. 3. Average SE and offloading probability w.r.t χ_1.

more MUs are associated with the MBSs with the raise of the SBS height and thus the spectral efficiency provided by MBSs, i.e., R_m, increases. However, since the increment of the R_m is neglectable compared with the decrease of R_s, the average sum SE achievable at mu, i.e., R, also decreases with the increase of H_1.

Fig. 3 shows the average SE *w.r.t* the cooperative distance threshold χ_1. It can be seen that with different SBS heights, the optimal cooperative distance threshold χ_1 always exists such that the average SE can be maximized, and the offloading probability increases with χ_i. When χ_1 is equal to the SBS height, i.e., $\chi_1 = H_1$, no SBSs can join to transmit the MUs' data. In such a scenario, all the SBSs are zero-loaded and the MUs are served by the nearest MBSs. As χ_1 grows, the area for candidate cooperative SBSs is expanded and thus the number of candidate SBSs is increased. Meanwhile, more MUs are offloaded to the SBSs and thus the cell load at SBSs becomes heavier, lowering the probability that a candidate SBSs participate in the cooperation. As a result, the average received signal strength first increases and then deteriorates with the increasing of χ_1. In addition, the interference caused by SBSs becomes more serious. When χ_1 is large enough, the SBSs are almost full-loaded with probability 1. In this scenario, the average SE and the offloading probability remain unchanged. Fig. 3 validates the theoretical analysis in Section V-B that there is a tradeoff between the number of candidate cooperative SBSs and the probability that an SBS participating the cooperation.

To further study the impact of the SBS height on the optimal χ_1, Fig. 4 shows the optimal χ_1 *w.r.t* to the SBS height H_1. It can be seen that the optimal χ_1 firstly decreases and then increases with the raise of SBS height while the maximum user SE $\mathcal{R}$ and the offloading probability decreases as SBS height increases. This is because the average SE provided by SBSs, i.e., $\mathcal{R}_s$, reduces while the average SE provided by MBSs, i.e., $\mathcal{R}_m$, increases with the raise of SBS height. As a result, shrinking the area for candidate cooperative SBSs can reduce the offloading probability and thus provide better SE, as the star-line in Fig. 4.

Fig. 5 presents the average SE *w.r.t* to the cache size L_1 to study the impact of the caching capability at SBSs. It shows that the offloading probability increases with the cache size at SBSs,

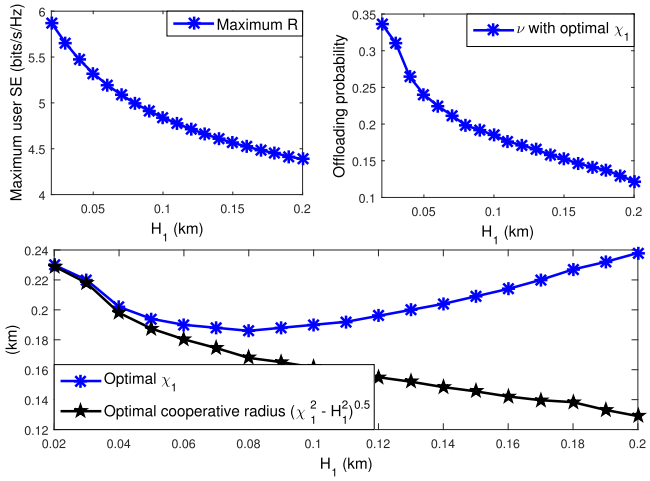

Fig. 4. Average SE and optimal χ_1 w.r.t the SBS height H_1.

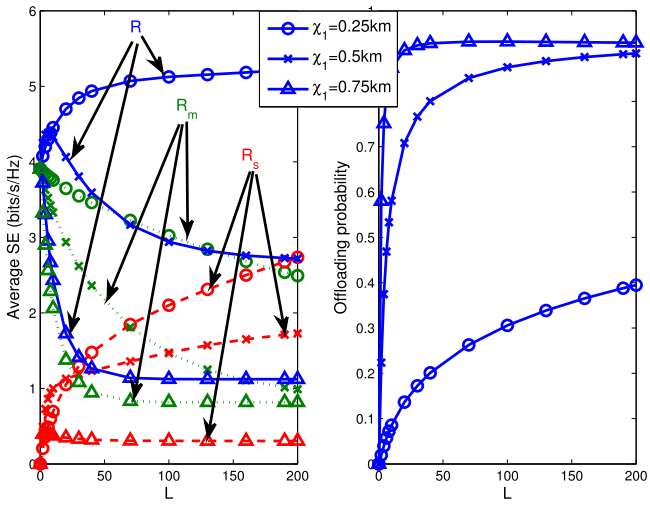

Fig. 5. Average SE and offloading probability w.r.t L_1, $\gamma = 0.2$.

while the optimal cache size exists in maximizing the average user SE ($\mathcal{R}$) and the average SE provided by SBSs ($\mathcal{R}_s$) with appropriate cooperative distance threshold. When the cooperative distance threshold χ_1 is 250 m and 500 m, the SBSs are light-loaded even with increasing L_1. In such a scenario, $\mathcal{R}_s$ increases with L_1 and finally reaches the maximum and levels off. However, when $\chi_1 = 500$ m, $\mathcal{R}$ exhibit a bell curve relationship *w.r.t* L_1 because the increase of $\mathcal{R}_s$ first dominates and then is dominated by the decrease of $\mathcal{R}_m$ with increasing L_1. As a result, the average user SE first improves and then decreases. With the expansion of the area for cooperative SBSs, such as $\chi_1 = 1000$ m, $\mathcal{R}_s$ first improves because the SBSs are mid-loaded, and then decreases because the SBSs become over-loaded. In such a scenario, the probability that an SBS participates the cooperation as well as the aggregated information signal strength firstly increases and then decreases with the increasing L_1, while the aggregated interference keeps increasing with the increase of L_1, which results in the bell curve of $\mathcal{R}_s$ *w.r.t* the L_1. It can be seen that if the cooperative distance threshold is too large, the MUs tend to be offloaded to far field SBSs with the increasing cache size and thus the SE decreases. In conclusion, we can see

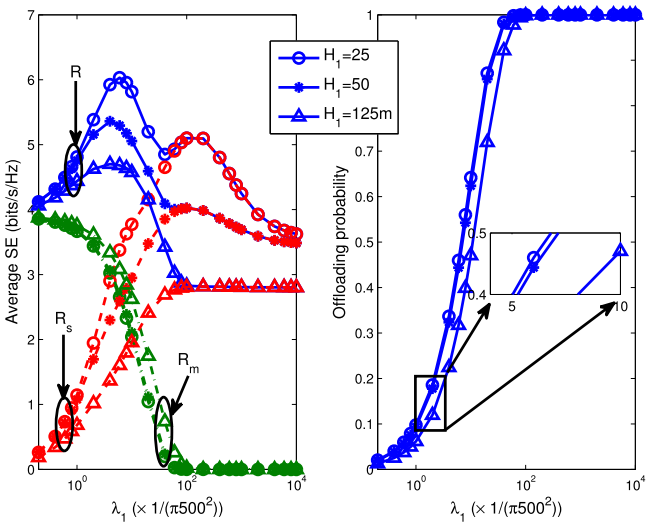

Fig. 6. Average SE w.r.t the SBS density λ_1, when $\chi_1 = 200$ m.

from Fig. 5 that the optimal cache size at SBSs depends on the determination of cooperative distance threshold χ_1.

Fig. 6 shows the average SE *w.r.t* the SBS density. It can be seen that the average SE ($\mathcal{R}_s$) exhibits a bell curve relationship *w.r.t.* the SBS density and thus the optimum SBS density exists in maximizing $\mathcal{R}_s$ and the average user SE ($\mathcal{R}$). With denser SBSs, more MUs are offloaded to the SBSs and finally all the MUs are associated the SBSs, as showed in the right-side figure. As a result, the average SE provided by the MBSs ($\mathcal{R}_m$) reduces and finally achieves zero. For the R_s, it firstly improves because more SBSs participate in the cooperation with the increasing SBS density, which results in the increase of the aggregated information signal strength. However, due to the limited area for cooperative SBSs, the increment in aggregate signal strength eventually reaches its limit and the R_s decreases due to the increase of received interference strength. Finally, the SE remains unchanged in an interference-limited scenario with increasing SBS density. Fig. 6 validate the theoretical analysis of Theorem 2.

With the MBS-assisted and content-aware cooperative transmission, the density of SBSs influences the number of cooperative SBS and the interfering SBSs, which further determines the optimal cooperative distance threshold χ_1. Fig. 7 depicts the maximum user SE $\mathcal{R}$ and the optimal χ_1 *w.r.t* to the SBS density. We can see that the optimal χ_1 decreases with the denser of SBSs and finally remains a minimum value greater than the SBS height. This is because with denser SBSs, the area for the cooperative SBSs shrinks to maintain the aggregated signal strength and meanwhile to reduce the aggregated interference strength.

VII. Conclusion

In this paper, we have investigated cooperative transmission in HetNets with cache-enabled SBSs, considering the impact of BS heights. An MBS-assisted and content-aware cooperative transmission strategy has been introduced to improve the spectral efficiency by offloading MUs from MBSs to the SBSs that can provide high data rate transmission. A new and accurate framework for the SE analysis has been formulated with a dual-slope path loss model. The explicit expressions for the SE have been derived with stochastic geometry. The analytical

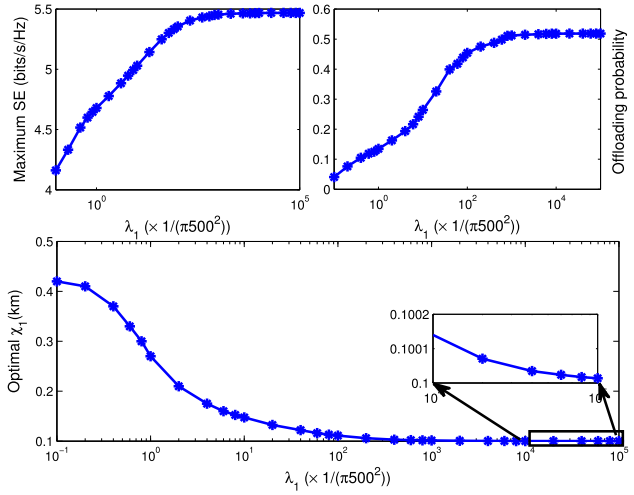

Fig. 7. Optimal χ_1 and maximum user SE w.r.t the SBS density λ_1, $H_1 = 100$ m.

results and the numerical analyses reveal that with the proposed cooperative transmission strategy, i) the SE decreases with increasing BS height; ii) the optimal cache size of SBSs providing the maximum SE reduces with the increase of the area for cooperative SBSs; iii) the optimal radius of area for candidate cooperative SBSs reduces with increasing SBS density and height. These results indicate that cooperative SBS cluster can enhance the network SE. However, the improvement of SE can be reduced with heavy-loaded SBS clusters due to the limited BS capacity. Moreover, load imbalance problem exists between the macrocell network and the small cell network if the SBSs are heavy-loaded. The analysis in this paper provide not only insights for the cooperative transmission in cache-enabled HetNets, but also the guidance for the optimization of network parameters. For the future work, we will study the joint optimization of cache size, BS density and cooperative distance threshold in HetNets to achieve the maximum network performance and load balancing between macrocell network and small cell networks.

Appendix A
Proof of Lemma 1

When $0 < r_0 \leqslant \sqrt{(d_{0,o})^2 - H_0^2}$, the Laplace function of I_0 is

$$\begin{aligned}
&\mathcal{L}_{I_0,1}(t|r_0) \\
&= \mathbb{E}_{I_0}\left[e^{-t\sum\limits_{x_{0,j}\in\Phi_0\setminus x_{0,0}} \mathbb{1}\left(m_{x_{0,j}}\geqslant 1\right)\frac{P_0^{(\mathrm{TX})}}{m}\, x_{0,j}\, l_0\left(\sqrt{|x_{0,j}|^2+H_0^2}\right)\|\mathbf{h}_j\|_2^2}\right] \\
&\overset{(e)}{=} \exp\left\{-2\pi\lambda_0\int_{r_0}^{\sqrt{(d_{0,o})^2-H_0^2}}\left(1-\left(1-\frac{\sqrt{x^2+H_0^2}}{d_{0,o}}\right)\right.\right. \\
&\quad\left.\left.\times\, \mathbb{E}_{\|\mathbf{h}\|_2^2,m}\left[e^{-\mathbb{1}(m\geqslant 1)\frac{tP_0^{(\mathrm{TX})}}{m}A_0^{(L)}\left(x^2+H_0^2\right)^{-\frac{\alpha_0^{(L)}}{2}}h}\right]-\frac{\sqrt{x^2+H_0^2}}{d_{0,o}}\right.\right. \\
&\quad\left.\left.\times\, \mathbb{E}_{\|\mathbf{h}\|_2^2,m}\left[e^{-\mathbb{1}(m\geqslant 1)\frac{tP_0^{(\mathrm{TX})}}{m}A_0^{(\mathrm{NL})}\left(x^2+H_0^2\right)^{-\frac{\alpha_0^{(\mathrm{NL})}}{2}}h}\right]\right)x\mathrm{d}x\right\} \\
&\quad\times\exp\left\{-2\pi\lambda_0\int_{\sqrt{(d_{0,o})^2-H_0^2}}^{\infty}(1\right. \\
&\quad\left.-\,\mathbb{E}_{\|\mathbf{h}\|_2^2,m}\left[e^{-\mathbb{1}(m\geqslant 1)\frac{tP_0^{(\mathrm{TX})}}{m}A_0^{(\mathrm{NL})}\left(x^2+H_0^2\right)^{-\frac{\alpha_0^{(\mathrm{NL})}}{2}}h}\right]\right)x\mathrm{d}x\Bigg\},
\end{aligned} \tag{49}$$

where (e) is the result of the path loss fading model (2). As discussed before, the channel fading gain between interfering MBS and the typical MU is gamma distribution with parameter m and 1, and the MBSs interferer the typical MU with probability $\sum_{m=1}^{M_0}\rho_0(m)$. Thus, (49) can be re-written as:

$$\begin{aligned}
&\mathcal{L}_{I_0,1}(t|r_0) \\
&= \exp\left\{-2\pi\lambda_0\sum_{m=1}^{M_0}\rho_0(m)\int_{r_0}^{\sqrt{(d_{0,o})^2-H_0^2}}\left(1-\frac{\sqrt{x^2+H_0^2}}{d_{0,o}}\right)\right. \\
&\quad\left.\times\left(1-\left(1+\frac{tP_0^{(\mathrm{TX})}}{m}A_0^{(\mathrm{L})}\left(x^2+H_0^2\right)^{-\frac{\alpha_0^{(\mathrm{L})}}{2}}\right)^{-m}\right)x\mathrm{d}x\right\} \\
&\quad\times\exp\left\{-2\pi\lambda_0\sum_{m=1}^{M_0}\rho_0(m)\int_{r_0}^{\sqrt{(d_{0,o})^2-H_0^2}}\frac{\sqrt{x^2+H_0^2}}{d_{0,o}}\right. \\
&\quad\left.\times\left(1-\left(1+\frac{tP_0^{(\mathrm{TX})}}{m}A_0^{(\mathrm{NL})}\left(x^2+H_0^2\right)^{-\frac{\alpha_0^{(\mathrm{NL})}}{2}}\right)^{-m}\right)x\mathrm{d}x\right\} \\
&\quad\times\exp\left\{-2\pi\lambda_0\sum_{m=1}^{M_0}\rho_0(m)\int_{\sqrt{(d_{0,o})^2-H_0^2}}^{\infty}(1\right. \\
&\quad\left.-\left(1+\frac{tP_0^{(\mathrm{TX})}}{m}A_0^{(\mathrm{NL})}\left(x^2+H_0^2\right)^{-\frac{\alpha_0^{(\mathrm{NL})}}{2}}\right)^{-m}\right)x\mathrm{d}x,\Bigg\}
\end{aligned} \tag{50}$$

where the first integral is

$$\begin{aligned}
&2\int_{r_0}^{\sqrt{(d_{0,o})^2-H_0^2}}\left(1-\frac{\sqrt{x^2+H_0^2}}{d_{0,o}}\right) \\
&\quad\times\left(1-\left(1+\frac{tP_0^{(\mathrm{TX})}}{m}A_0^{(L)}\left(x^2+H_0^2\right)^{-\frac{\alpha_0^{(L)}}{2}}\right)^{-m}\right)x\mathrm{d}x \\
&= \mathcal{Z}\left(\alpha_0^{(L)},m,2,m,P_0^{(\mathrm{TX})}A_0^{(L)},d_{0,o}\right) \\
&\quad-\mathcal{Z}\left(\alpha_0^{(L)},m,2,m,P_0^{(\mathrm{TX})}A_0^{(L)},\sqrt{r_0^2+H_0^2}\right) \\
&\quad-\frac{2}{3}\mathcal{Z}\left(\alpha_0^{(L)},m,3,m,P_0^{(\mathrm{TX})}A_0^{(L)},d_{0,o}\right) \\
&\quad+\frac{2\sqrt{r_0^2+H_0^2}}{3d_{0,o}}\mathcal{Z}\left(\alpha_0^{(L)},m,3,m,P_0^{(\mathrm{TX})}A_0^{(L)},\sqrt{r_0^2+H_0^2}\right).
\end{aligned} \tag{51}$$

The second integral is

$$2\int_{r_0}^{\sqrt{(d_{0,o})^2-H_0^2}} \frac{\sqrt{x^2+H_0^2}}{d_{0,o}} \times \left(1-\left(1+\frac{tP_0^{(\mathrm{TX})}}{m}A_0^{(\mathrm{NL})}\left(x^2+H_0^2\right)^{-\frac{\alpha_0^{(\mathrm{NL})}}{2}}\right)^{-m}\right)x\mathrm{d}x$$
$$=\frac{2}{3}\mathcal{Z}\left(\alpha_0^{(\mathrm{NL})},m,3,m,P_0^{(\mathrm{TX})}A_0^{(\mathrm{NL})},d_{0,o}\right) -\frac{2\sqrt{r_0^2+H_0^2}}{3d_{0,o}}\mathcal{Z}\left(\alpha_0^{(\mathrm{NL})},m,3,m,P_0^{(\mathrm{TX})}A_0^{(\mathrm{NL})},\sqrt{r_0^2+H_0^2}\right). \tag{52}$$

and the last integral is

$$\begin{aligned}&2\int_{\sqrt{(d_{0,o})^2-H_0^2}}^{\infty}\left(1-\left(1+\frac{tP_0^{(\mathrm{TX})}A_0^{(\mathrm{NL})}}{m}\left(x^2+H_0^2\right)^{-\frac{\alpha_0^{(\mathrm{NL})}}{2}}\right)^{-m}\right)x\mathrm{d}x\\ &\overset{(f)}{=}\infty^2-(d_{0,o})^2-\frac{2}{\alpha_0^{(\mathrm{NL})}}\left(\frac{tP_0^{(\mathrm{TX})}A_0^{(\mathrm{NL})}}{m}\right)^{\frac{2}{\alpha_0^{(\mathrm{NL})}}}\\ &\times\int_{\frac{m}{tP_0^{(\mathrm{tx})}A_0^{(\mathrm{NL})}}(d_{0,o})^{\alpha_0^{(\mathrm{NL})}}}^{\infty}\frac{z^{m+\frac{2}{\alpha_0^{(\mathrm{NL})}}-1}}{(1+z)^m}\mathrm{d}z\\ &=\infty^2-\mathcal{Z}\left(\alpha_0^{(\mathrm{NL})},m,2,m,P_0^{(\mathrm{TX})}A_0^{(\mathrm{NL})},d_{0,o}\right)\end{aligned} \tag{53}$$

where (*f*) is obtained by setting

$$z=\frac{m}{tP_0^{(\mathrm{TX})}A_0^{(\mathrm{NL})}}\left(x^2+H_0^2\right)^{\frac{\alpha_0^{(\mathrm{NL})}}{2}}.$$

Substituting (51)–(53) into (50), the Laplace function of I_0 with $0<r_0\leqslant\sqrt{(d_{0,o})^2-H_0^2}$ is obtained as (28).

When $r_0>\sqrt{(d_{0,o})^2-H_0^2}$, the Laplace function of I_0 is

$$\mathcal{L}_{I_{0,2}}(t|r_0)=\exp\left\{-2\pi\lambda_0\int_{r_0}^{\infty}(1-\mathbb{E}_{\|\mathbf{h}\|_2^2,m}\left[e^{-\mathbb{1}(m\geqslant 1)\frac{tP_0^{(\mathrm{TX})}A_0^{(\mathrm{NL})}}{m}(x^2+H_0^2)^{-\frac{\alpha_0^{(\mathrm{NL})}}{2}}\|\mathbf{h}\|_2^2}\right])x\mathrm{d}x\right\}$$
$$=\exp\left\{\begin{aligned}&-2\pi\lambda_0\textstyle\sum_{m=1}^{M_0}\rho_0(m)\times\\ &\int_{r_0}^{\infty}\left(1-\left(1+\frac{tP_0^{(\mathrm{TX})}A_0^{(\mathrm{NL})}}{m}(x^2+H_0^2)^{-\frac{\alpha_0^{(\mathrm{NL})}}{2}}\right)^{-m}\right)x\mathrm{d}x\end{aligned}\right\} \tag{54}$$

With the similar derivation process as (53), $\mathcal{L}_{I_{0,2}}(t|r_0)$ can be obtained as (31).

Appendix B
Proof of Lemma 2

When $0<\chi_k\leqslant d_{k,o}$, the Laplace function of S_k is given in (55), as shown at the top of the next page, where (g) is the result of the picewise modeling of path loss fading and the fact that an SBS participates in cooperation with probability ϕ_k. Since $\|\mathbf{h}\|_2^2\triangleq\|\mathbf{h}_{x_{k,i}}\|_2^2$ follows the gamma distribution $\Gamma(N_k-n_k,1)$, the expectation over $\|\mathbf{h}\|_2^2$ is

$$\mathbb{E}_{\|\mathbf{h}\|_2^2}[e^{-ah}]=\frac{1}{(a+1)^{N_k-m_k}}.$$

Therefore, the Laplace function of S_k can be obtained as (34) by applying the similar manipulations as (51) and (52).

Similarly, when $H_k<d_{k,o}<\chi_k$, the integration in $\mathcal{L}_{S_k}(t)$ should be divided into slots $(0,\sqrt{(d_{k,o})^2-H_k^2})$ and $(\sqrt{(d_{k,o})^2-H_k^2},\sqrt{\chi_k^2-H_k^2})$. The signals within $(0,\sqrt{(d_{k,o})^2-H_k^2})$ pass though NLoS and LoS with probability $\frac{\sqrt{x^2+H_k^2}}{d_{k,o}}$ and $(1-\frac{\sqrt{x^2+H_k^2}}{d_{k,o}})$, respectively. And they go through NLoS with probability 1 in $(\sqrt{(d_{k,o})^2-H_k^2},\sqrt{\chi_k^2-H_k^2})$. With further derivation and the same manipulation as (51) and (52), the Laplace function of S_k under the case $H_k<d_{k,o}<\chi_k$ is obtained as (36). When $d_{k,o}<H_k<\chi_k$, the signals go NLoS with probability 1 in the whole area for the cooperative SBSs in the k-th tier and thus $\mathcal{L}_{S_k}(t)$ is obtained as (37).

Appendix C
Proof of Lemma 3

The analysis of $\mathcal{L}_{I_{k,\mathrm{in}}}(t)$ can be easily extended with the result of $\mathcal{L}_{S_k}(t)$ by i) replacing the cooperating probability ϕ_k with interfering probability $(1-\eta_k)\sum_{m_k=1}^{M_k-1}\rho_k(m_k+1)+\sum_{m_k=M_k}^{\infty}p_k(m_k+1)(1-\frac{\eta_k M_k}{m_k+1})$, ii) replacing $\frac{P_k^{(\mathrm{TX})}}{n_k+1}$ with $\frac{P_k^{(\mathrm{TX})}}{m_k}$, and iii) applying the interfering channel fading $\|\mathbf{h}\|_2^2\sim\Gamma(m_k,1)$.

When $0<\chi_k\leqslant d_{k,o}$, the Laplace function of $I_{k,\mathrm{out}}$ can be calculated as:

$$\mathcal{L}_{I_{k,\mathrm{out}}}(t)=\exp\left\{\begin{aligned}&-2\pi\lambda_k\sum_{m_k=1}^{M_k}\rho_k(m_k)\int_{\sqrt{\chi_k^2-H_k^2}}^{\sqrt{(d_{k,o})^2-H_k^2}}\left(1-\frac{\sqrt{x^2+H_k^2}}{d_{k,o}}\right)\\ &\times\left(1-\mathbb{E}_{\left\|\mathbf{h}_{x_{k,i}}\right\|_2^2}\left[e^{-\frac{P_k^{(\mathrm{TX})}A_k^{(L)}}{m_k}\left(x^2+H_k^2\right)^{-\frac{\alpha_k^{(L)}}{2}}h}\right]\right)x\mathrm{d}x\end{aligned}\right\}$$
$$\times\exp\left\{\begin{aligned}&-2\pi\lambda_k\sum_{m_k=1}^{M_k}\rho_k(m_k)\int_{\sqrt{\chi_k^2-H_k^2}}^{\sqrt{(d_{k,o})^2-H_k^2}}\frac{\sqrt{x^2+H_k^2}}{d_{k,o}}\\ &\times\left(1-\mathbb{E}_{\left\|\mathbf{h}_{x_{k,i}}\right\|_2^2}\left[e^{-\frac{P_k^{(\mathrm{TX})}}{m_k}A_k^{(\mathrm{NL})}\left(x^2+H_k^2\right)^{-\frac{\alpha_k^{(\mathrm{NL})}}{2}}h}\right]\right)x\mathrm{d}x\end{aligned}\right\}$$

$$\mathcal{L}_{S_k}(t)=\mathbb{E}_{\Phi_k}\left[\exp\left\{-t\sum_{x_{k,i}\in\Phi_k\cap\mathcal{B}\left(0,\sqrt{\chi_k^2-H_k^2}\right)}\mathbf{1}\left(E_2\ \&\ E_3\right)\frac{P_k^{(\mathrm{TX})}}{m_{x_{k,i}}+1}l_k\left(\sqrt{|x_{k,i}|^2+H_k^2}\right)\left\|\mathbf{h}_{x_{k,i}}\right\|_2^2\right\}\right]$$

$$\overset{(g)}{=}\exp\left\{\begin{array}{l}-2\pi\lambda_k\eta_k\left(\sum_{n_k=0}^{M_k-1}p_k\left(n_k+1\right)\int_0^{\sqrt{\chi_k^2-H_k^2}}\left(1-\frac{\sqrt{x^2+H_k^2}}{d_{k,o}}\right)\left(1-\mathbb{E}_{\left\|\mathbf{h}_{x_{k,i}}\right\|_2^2}\left[e^{-\frac{P_k^{(\mathrm{TX})}A_k^{(\mathrm{L})}}{n_k+1}\left(x^2+H_k^2\right)^{-\frac{\alpha_k^{(\mathrm{L})}}{2}}h}\right]\right)x\mathrm{d}x\right.\\ \left.+\sum_{n_k=M_k}^{\infty}\frac{p_k\left(n_k+1\right)M_k}{n_k+1}\int_0^{\sqrt{\chi_k^2-H_k^2}}\left(1-\frac{\sqrt{x^2+H_k^2}}{d_{k,o}}\right)\left(1-\mathbb{E}_{\left\|\mathbf{h}_{x_{k,i}}\right\|_2^2}\left[e^{-\frac{P_k^{(\mathrm{TX})}A_k^{(\mathrm{L})}}{M_k}\left(x^2+H_k^2\right)^{-\frac{\alpha_k^{(\mathrm{L})}}{2}}h}\right]\right)x\mathrm{d}x\right)\end{array}\right\}$$

$$\times\exp\left\{\begin{array}{l}-2\pi\lambda_k\eta_k\left(\sum_{n_k=0}^{M_k-1}p_k\left(n_k+1\right)\int_0^{\sqrt{\chi_k^2-H_k^2}}\frac{\sqrt{x^2+H_k^2}}{d_{k,o}}\left(1-\mathbb{E}_{\left\|\mathbf{h}_{x_{k,i}}\right\|_2^2}\left[e^{-\frac{P_k^{(\mathrm{TX})}}{n_k+1}A_k^{(\mathrm{NL})}\left(x^2+H_k^2\right)^{-\frac{\alpha_k^{(\mathrm{NL})}}{2}}h}\right]\right)x\mathrm{d}x\right.\\ \left.+\sum_{n_k=M_k}^{\infty}\frac{p_k\left(n_k+1\right)M_k}{n_k+1}\int_0^{\sqrt{\chi_k^2-H_k^2}}\frac{\sqrt{x^2+H_k^2}}{d_{k,o}}\left(1-\mathbb{E}_{\left\|\mathbf{h}_{x_{k,i}}\right\|_2^2}\left[e^{-\frac{P_k^{(\mathrm{TX})}}{M_k}A_k^{(\mathrm{NL})}\left(x^2+H_k^2\right)^{-\frac{\alpha_k^{(\mathrm{NL})}}{2}}h}\right]\right)x\mathrm{d}x\right)\end{array}\right\} \tag{55}$$

$$\times\exp\left\{\begin{array}{l}-2\pi\lambda_k\sum_{m_k=1}^{M_k}\rho_k\left(m_k\right)\int_{\sqrt{\left(d_{k,o}\right)^2-H_k^2}}^{\infty}\left(1-\right.\\ \left.\mathbb{E}_{\left\|\mathbf{h}_{x_{k,i}}\right\|_2^2}\left[e^{-\frac{P_k^{(\mathrm{TX})}}{m_k}A_k^{(\mathrm{NL})}\left(x^2+H_k^2\right)^{-\frac{\alpha_k^{(\mathrm{NL})}}{2}}h}\right]\right)x\mathrm{d}x\end{array}\right\}, \tag{56}$$

which can be calculated with the same derivation process as in (50). After further derivation and manipulation, $\mathcal{L}_{I_{k,\mathrm{out}}}(t)$ can be obtained as (41).

When $\chi_k > d_{k,o}$, only NLoS occurs for the interference outside $\mathcal{B}(0,\chi_k)$ and therefore NLoS exists with probability 1 in the integration space of $\mathcal{L}_{I_{k,\mathrm{out}}}(t)$. The detailed proof of the case $\chi_k > d_{k,o}$ can be extended with the derivation process of (56).

REFERENCES

[1] A. Damnjanovic *et al.*, "A survey on 3GPP heterogeneous networks," *IEEE Wireless Commun.*, vol. 18, no. 3, pp. 10–21, Jun. 2011.

[2] N. Zhang, N. Cheng, A. Gamage, K. Zheng, J. W. Mark, and X. Shen, "Cloud assisted HetNets toward 5G wireless networks," *IEEE Commun. Mag.*, vol. 53, no. 6, pp. 59–65, Jun. 2015.

[3] M. Zhang, H. Luo, and H. Zhang, "A survey of caching mechanisms in information-centric networking," *IEEE Commun. Surveys Tuts.*, vol. 17, no. 3, pp. 1473–1499, Third Quarter 2015.

[4] G. Paschos, E. Baştuğ, I. Land, G. Caire, and M. Debbah, "Wireless caching: Technical misconceptions and business barriers," *IEEE Commun. Mag.*, vol. 54, no. 8, pp. 16–22, Aug. 2016.

[5] S. Zhang, N. Zhang, X. Fang, P. Yang, and X. Shen, "Self-sustaining caching stations: Toward cost-effective 5G-enabled vehicular networks," *IEEE Commun. Mag.*, vol. 55, no. 11, pp. 202–208, Nov. 2017.

[6] H. Zhang, Y. Qiu, X. Chu, K. Long, and V. Leung, "Fog radio access networks: Mobility management, interference mitigation and resource optimization," *arXiv preprint arXiv: 1707.06892*, 2017.

[7] X. Li, X. Wang, K. Li, Z. Han, and V. C. Leung, "Collaborative multi-tier caching in heterogeneous networks: Modeling, analysis, and design," *IEEE Trans. Wireless Commun.*, vol. 16, no. 10, pp. 6926–6939, Oct. 2017.

[8] Y. Zhou, F. R. Yu, J. Chen, and Y. Kuo, "Resource allocation for information-centric virtualized heterogeneous networks with in-network caching and mobile edge computing," *IEEE Trans. Veh. Technol.*, vol. 66, no. 12, pp. 11339–11351, Dec. 2017.

[9] Y. Chen, M. Ding, J. Li, Z. Lin, G. Mao, and L. Hanzo, "Probabilistic small-cell caching: Performance analysis and optimization," *IEEE Trans. Veh. Technol.*, vol. 66, no. 5, pp. 4341–4354, May 2017.

[10] S. Zhang, N. Zhang, P. Yang, and X. S. Shen, "Cost-effective cache deployment in mobile heterogeneous networks," *IEEE Trans. Veh. Technol.*, vol. 66, no. 12, pp. 11264–11276, Dec. 2017.

[11] B. Han, X. Wang, N. Choi, T. Kwon, and Y. Choi, "AMVS-NDN: Adaptive mobile video streaming and sharing in wireless named data networking," in *Proc. IEEE Conf. Comput. Commun. Workshops*, Apr. 2013, pp. 375–380.

[12] Z. Chen, J. Lee, T. Q. Quek, and M. Kountouris, "Cooperative caching and transmission design in cluster-centric small cell networks," *IEEE Trans. Wireless Commun.*, vol. 16, no. 5, pp. 3401–3415, May 2017.

[13] H. Zhang, C. Jiang, J. Cheng, and V. C. Leung, "Cooperative interference mitigation and handover management for heterogeneous cloud small cell networks," *IEEE Wireless Commun.*, vol. 22, no. 3, pp. 92–99, Jun. 2015.

[14] A. Liu and V. K. Lau, "Cache-enabled opportunistic cooperative MIMO for video streaming in wireless systems," *IEEE Trans. Signal Processing*, vol. 62, no. 2, pp. 390–402, Jan. 2014.

[15] W. Wen, Y. Cui, F.-C. Zheng, S. Jin, and Y. Jiang, "Random caching based cooperative transmission in heterogeneous wireless networks," *arXiv preprint arXiv: 1701.05761*, 2017.

[16] N. Golrezaei, K. Shanmugam, A. G. Dimakis, A. F. Molisch, and G. Caire, "Femtocaching: Wireless video content delivery through distributed caching helpers," in *Proc. IEEE Conf. Conf. Comput. Commun.*, Mar. 2012, pp. 1107–1115.

[17] E. Baştuğ, M. Debbah, M. Kountouris, and M. Bennis, "Cache-enabled small cell networks: Modeling and tradeoffs," *EURASIP J. Wireless Commun. Netw.*, vol. 2015, no. 1, Dec. 2015, Art. no. 41.

[18] C. Yang, Y. Yao, Z. Chen, and B. Xia, "Analysis on cache-enabled wireless heterogeneous networks," *IEEE Trans. Wireless Commun.*, vol. 15, no. 1, pp. 131–145, Jan. 2016.

[19] J. Liu and S. Sun, "Energy efficiency analysis of cache-enabled cooperative dense small cell networks," *IET Commun.*, vol. 11, no. 4, pp. 477–482, Mar. 2017.

[20] Y. Liu, C. Yang, Y. Yao, B. Xia, Z. Chen, and X. Li, "Interference management in cache-enabled stochastic networks: A content diversity approach," *IEEE Access*, vol. 5, pp. 1609–1617, 2017.
[21] B. Blaszczyszyn and A. Giovanidis, "Optimal geographic caching in cellular networks," in *Proc. IEEE Int. Conf. Commun.*, Jun. 2015, pp. 3358–3363.
[22] X. Zhang and J. G. Andrews, "Downlink cellular network analysis with multi-slope path loss models," *IEEE Trans. Commun.*, vol. 63, no. 5, pp. 1881–1894, May 2015.
[23] M. Ding, P. Wang, D. López-Pérez, G. Mao, and Z. Lin, "Performance impact of LOS and NLOS transmissions in dense cellular networks," *IEEE Trans. Wireless Commun.*, vol. 15, no. 3, pp. 2365–2380, Mar. 2016.
[24] I. Atzeni, J. Arnau, and M. Kountouris, "Downlink cellular network analysis with LOS/NLOS propagation and elevated base stations," *arXiv preprint arXiv: 1703.01279*, 2017.
[25] M. Haenggi, *Stochastic Geometry for Wireless Networks*. Cambridge, U.K.: Cambridge Univ. Press, 2012.
[26] N. Zhang, S. Zhang, S. Wu, J. Ren, J. W. Mark, and X. Shen, "Beyond coexistence: Traffic steering in LTE networks with unlicensed bands," *IEEE Wireless Commun.*, vol. 23, no. 6, pp. 40–46, Dec. 2016.
[27] X. Wang, M. Chen, T. Taleb, A. Ksentini, and V. C. M. Leung, "Cache in the air: Exploiting content caching and delivery techniques for 5G systems," *IEEE Trans. Commun.*, vol. 52, no. 2, pp. 131–139, Feb. 2014.
[28] Spatial Channel Model AHG, "Subsection 3.5.3, spatial channel model text description," V6.0, Apr. 2003. [Online]. Available: http://ftp://www.3gpp.org/tsg_ran/WG1_RL1/3GPP_3GPP2_SCM/$ConfCall-16-20030417$/$ SCM-134/%20Text/%20v$6.0.zip
[29] COST Action 231, "Digital mobile radio towards future generation systems," European Communities, EUR, Tech. Rep. 18957, 1999.
[30] G. Liu, Z. Ma, X. Chen, Z. Ding, R. Yu, and P. Fan, "Cross-layer power allocation in non-orthogonal multiple access systems for statistical QoS provisioning," *IEEE Trans. Veh. Technol.*, vol. 66, no. 12, pp. 11388–11393, Dec. 2017.
[31] N. Jindal, J. G. Andrews, and S. Weber, "Multi-antenna communication in Ad hoc networks: Achieving MIMO gains with SIMO transmission," *IEEE Trans. Commun.*, vol. 59, no. 2, pp. 529–540, Feb. 2011.
[32] C. Li, J. Zhang, J. G. Andrews, and K. B. Letaief, "Success probability and area spectral efficiency in multiuser MIMO HetNets," *IEEE Trans. Commun*, vol. 64, no. 4, pp. 1544–1556, Apr. 2016.
[33] J.-S. Ferenc and Z. Néda, "On the size distribution of poisson voronoi cells," *Phys. A: Statist. Mech. Appl.*, vol. 385, no. 2, pp. 519–529, 2007.
[34] T. Kiang, "Random fragmentation in two and three dimensions," *Zeitschrift Astrophysik*, vol. 64, pp. 433–439, Jun. 1966.
[35] K. A. Hamdi, "A useful lemma for capacity analysis of fading interference channels," *IEEE Trans. Commun.*, vol. 58, no. 2, pp. 411–416, Feb. 2010.
[36] H. Robert W, M. Kountouris, and T. Bai, "Modeling heterogeneous network interference using poisson point processes," *IEEE Trans. Signal Process.*, vol. 61, no. 16, pp. 4114–4126, Aug. 2013.
[37] H. S. Dhillon, R. K. Ganti, F. Baccelli, and J. G. Andrews, "Modeling and analysis of k-tier downlink heterogeneous cellular networks," *IEEE J. Sel. Areas Commun.*, vol. 30, no. 3, pp. 550–560, Mar. 2012.
[38] S. Mukherjee, "Distribution of downlink SINR in heterogeneous cellular networks," *IEEE J. Sel. Areas Commun.*, vol. 30, no. 3, pp. 575–585, Apr. 2012.
[39] H. Wu, N. Zhang, X. Tao, Z. Wei, and X. Shen, "Capacity-and trust-aware bs cooperation in non-uniform HetNets: Spectral efficiency and optimal BS density," *IEEE Trans. Veh. Technol.*, vol. 66, no. 12, pp. 11317–11329, Dec. 2017.
[40] 3GPP, "Further enhancements to LTE time division duplex (TDD) for downlink-uplink (DL-UL) interference management and traffic adaptation," European Communities, EUR, Tech. Rep. 36.828 (v11.0.0), Jun. 2012.

Huici Wu received the B.S. degree in information engineering from the Communication University of China, Beijing, China, in 2013. She is currently working toward the Ph.D. degree from Beijing University of Posts and Telecommunications, Beijing. From September 2016 to August 2017, she was a Visiting Researcher with the Broadband Communications Research Group, Department of Electrical and Computer Engineering, University of Waterloo, Waterloo, ON, Canada. Her research interests include wireless communications and networks, with an emphasis on the coordinated multipoint and physical layer security in heterogeneous networks.

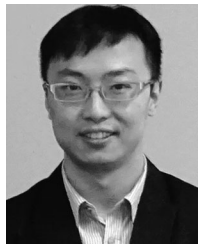

Ning Zhang (M'15) received the Ph.D. degree from the University of Waterloo, Waterloo, ON, Canada, in 2015. He is currently an Assistant Professor with the Department of Computing Science, Texas A&M University–Corpus Christi, Corpus Christi, TX, USA. Before that, he was a Postdoctoral Research Fellow with the Broadband Communications Research Group, University of Waterloo. His current research interests include next-generation wireless networks, software-defined networking, vehicular networks, and physical layer security. He was the co-recipient of the Best Paper Award at the 2014 IEEE Global Communications Conference and the 2015 IEEE International Conference on Wireless Communications and Signal Processing.

Zhiqing Wei (S'12–M'15) received the B.S. and Ph.D. degrees from the Beijing University of Posts and Telecommunications (BUPT), Beijing, China, in 2010 and 2015, respectively. He is currently a Lecturer with BUPT. He has authored or coauthored two books and chapters and more than 30 journal and conferences papers. His research interests include the optimization and performance analysis of cognitive radio networks, mobile social networks, and unmanned aerial vehicle networks. He is a Reviewer for the IEEE COMMUNICATIONS MAGAZINE, the IEEE TRANSACTIONS ON VEHICULAR TECHNOLOGY, and the IEEE COMMUNICATIONS LETTERS.

Shan Zhang (S'13–M'16) received the B.S. degree in information from the Beijing Institute of Technology, Beijing, China, in 2011, and the Ph.D. degree in electronic engineering from Tsinghua University, Beijing, in 2016. She is currently at the School of Computer Science and Engineering, Beihang University, Beijing. From August 2016 to December 2017, she was a Postdoctoral Fellow with the Department of Electronic and Computer Engineering, University of Waterloo, Waterloo, ON, Canada. Her research interests include network resource and traffic management, network visualization, and integration. She was a recipient of the Best Paper Award at the Asia-Pacific Conference on Communication in 2013.

Xiaofeng Tao (SM'13) received the B.S. degree in electrical engineering from Xi'an Jiaotong University, Xi'an, China, in 1993, and the M.S.E.E. and Ph.D. degrees in telecommunication engineering from the Beijing University of Posts and Telecommunications (BUPT), Beijing, China, in 1999 and 2002, respectively. He was a Visiting Professor with Stanford University, Stanford, CA, USA, from 2010 to 2011, the Chief Architect of the Chinese National FuTURE Fourth-Generation (4G) TDD working group from 2003 to 2006, and established the 4G TDD CoMP trial network in 2006. He is currently a Professor with the BUPT. He is the inventor or coinventor of 50 patents and the author or coauthor of 120 papers in 4G and beyond 4G. He is a Fellow of the Institution of Engineering and Technology.

Xuemin Shen (M'97–SM'02–F'09) received the Ph.D. degree from Rutgers University, New Brunswick, NJ, USA, in 1990. He is currently a University Professor with the Department of Electrical and Computer Engineering, University of Waterloo, Waterloo, ON, Canada. His research interests include resource management in interconnected wireless/wired networks, wireless network security, social networks, smart grid, and vehicular ad hoc and sensor networks. He served as the Technical Program Committee Chair/Co-Chair for the 2016 IEEE Global Communications Conference, the 2014 IEEE Conference on Computer Communications, the 2010 IEEE Vehicular Technology Conference, Fall, and the 2007 IEEE Global Communications Conference, and the Symposia Chair for the 2010 IEEE International Conference on Communications. He also serves as the Editor-in-Chief for the IEEE INTERNET OF THINGS JOURNAL, PEER-TO-PEER NETWORKING AND APPLICATION, and IET COMMUNICATIONS, and a Founding Area Editor for the IEEE TRANSACTIONS ON WIRELESS COMMUNICATIONS. He received the Excellent Graduate Supervision Award in 2006, the Outstanding Performance Award in 2004, 2007, 2010, and 2014 from the University of Waterloo, the Premiers Research Excellence Award in 2003 from the Province of Ontario, Canada, the Distinguished Performance Award in 2002 and 2007 from the Faculty of Engineering, University of Waterloo, the Joseph LoCicero Award, and the Education Award 2017 from the IEEE Communications Society. He is a registered Professional Engineer of Ontario, Canada, a Fellow of the Engineering Institute of Canada, the Canadian Academy of Engineering, and the Royal Society of Canada, and a Distinguished Lecturer of the IEEE Vehicular Technology Society and IEEE Communications Society.

Ping Zhang received the M.S. degree in electrical engineering from Northwestern Polytechnical University, Xi'an, China, in 1986, and the Ph.D. degree in electric circuits and systems from the Beijing University of Posts and Telecommunications (BUPT), Beijing, China, in 1990. He is currently a Professor with BUPT, where he is the Director of the State Key Laboratory of Networking and Switching Technology. His research interests include cognitive wireless networks, fourth-generation mobile communication, fifth-generation mobile networks, communications factory test instruments, universal wireless signal detection instruments, and mobile Internet.

Dr. Zhang is the Executive Associate Editor-in-Chief on information sciences of the *Chinese Science Bulletin*, a Guest Editor for the IEEE WIRELESS COMMUNICATIONS MAGAZINE, and an Editor of *China Communications*. He was a recipient of the First and Second Prizes from the National Technology Invention and Technological Progress Awards, as well as the First Prize Outstanding Achievement Award of Scientific Research in College.